Orogenic eclogites record relative magnitude of deep crustal flow and extent of migmatite-eclogite interaction

Clémentine Hamelin, Donna L. Whitney, Françoise Roger, Christian Teyssier

▶ **To cite this version:**

Clémentine Hamelin, Donna L. Whitney, Françoise Roger, Christian Teyssier. Orogenic eclogites record relative magnitude of deep crustal flow and extent of migmatite-eclogite interaction. Lithos, In press, 10.1016/j.lithos.2022.106917 . hal-03828760v1

HAL Id: hal-03828760

https://hal.umontpellier.fr/hal-03828760v1

Submitted on 25 Oct 2022 (v1), last revised 2 Nov 2022 (v2)

HAL is a multi-disciplinary open access archive for the deposit and dissemination of scientific research documents, whether they are published or not. The documents may come from teaching and research institutions in France or abroad, or from public or private research centers.

L'archive ouverte pluridisciplinaire **HAL**, est destinée au dépôt et à la diffusion de documents scientifiques de niveau recherche, publiés ou non, émanant des établissements d'enseignement et de recherche français ou étrangers, des laboratoires publics ou privés.

Manuscript

Click here to view linked References

Click here to access/download;Manuscript;2022_Hamelin_etal_Lithos_MNeclo

Orogenic eclogites record relative magnitude of deep crustal flow and extent of migmatite-eclogite interaction

Hamelin, Clémentine (hamel038@umn.edu)[a]

Whitney, Donna L. (dwhitney@umn.edu)[a]

Roger, Françoise (francoise.roger@umontpellier.fr)[b]

Teyssier, Christian (teyssier@umn.edu)[a]

[a] Department of Earth and Environmental Sciences, University of Minnesota, Minneapolis, MN 55455, USA

[b] Laboratoire Géosciences Montpellier (CNRS-UMR 5243), Université Montpellier, 34095 Montpellier Cedex 5, France

Corresponding author:

Clémentine Hamelin (email: hamel038@umn.edu)

Permanent address:

Department of Earth and Environmental Sciences,
University of Minnesota – Twin-Cities,
John T. Tate Hall room 150,
116 Church St SE,
Minneapolis, MN 55455, USA

Word count (introduction to conclusion + figure, table captions): 9,513

Abstract

In exhumed orogens, refractory mafic rocks have the potential to preserve a record of petrogenesis and high-pressure (H*P*) metamorphism that is commonly obliterated in quartzofeldspathic rocks owing to re-equilibration at high-temperature, low-pressure (H*T*-L*P*) conditions. In the Montagne Noire (France) migmatite dome, located in the foreland of the Variscan orogen, eclogite is exposed in both the core and margin of the dome. In this study, we combine *in situ* U-Pb petrochronology and oxygen-isotope analyses of key eclogite phases to demonstrate that the eclogites had different protoliths and source regions, traveled variable distances laterally in the deep crust, and differentially interacted with surrounding migmatite prior to exhumation. Dome-margin eclogite zircons are small (~40 μm) with well-preserved inherited cores and thin (<15 μm) rims, compared to larger (40-120 μm) neo- and recrystallized dome-core zircons with small relict cores and wide (15-30 μm) recrystallized rims. Protolith and H*P* metamorphism ages were determined using *in situ* zircon and rutile petrochronology (LASS-ICP-MS). Both eclogites formed in a continental setting; dome margin protolith zircon cores formed at 442.5 ± 3.4 Ma (steep HREE slope, no Eu-anomaly) whereas zircon cores of the dome-core eclogites yielded scattered dates suggesting protolith crystallization between ~500–400 Ma (steep HREE slope, pronounced Eu-anomaly). Both eclogites experienced H*P* metamorphism at *c.* 320–310 Ma in garnet-stable, plagioclase-absent conditions. Most analyzed rutile yielded dates of 307-304 Ma associated with cooling. The record of H*P* fluid conditions was determined by O-isotope (SIMS) analyses of garnet and zircon. Dome-margin zircon cores and rims have $\delta^{18}O$ of ~8.2-8.5 ‰, indistinguishable within uncertainty, in isotopic equilibrium with isotopically unzoned garnet ($\delta^{18}O$ ~8.0-8.2 ‰). In contrast, zircons in dome-core eclogites have systematically lower zircon-core $\delta^{18}O$ values compared to their rims and neocrystallized

grains, and zircon cores are in equilibrium with major-cation zoned garnet $\delta^{18}O$. The two dome-core eclogite samples yielded zircon and garnet yield $\delta^{18}O$ values ~8.6-9.5 ‰ and ~9.7-10.5 ‰. Based on these results, we propose that (1) protolith gabbro for the two eclogites were emplaced at different depths in a Cambro-Ordovician continental crustal package; and (2) dome-core eclogites interacted extensively with surrounding gneiss during burial accompanied by foreland-vergent crustal flow, whereas the dome-margin eclogite was sourced proximally to the dome emplacement location after eclogitization and had minimal interaction with surrounding gneiss prior to exhumation. This study shows that a multi-method, multi-systems approach to studying eclogite in migmatite domes can be used to evaluate the magnitude and trajectory of deep orogenic crustal flow. At least parts of the Montagne Noire migmatite dome are deeply sourced, but rocks exhumed in the core had a more extensive and protracted history of deep-crustal flow than deep-crustal rocks exhumed at the margin.

Keywords: deep crust, eclogite, fluid-rock interactions, U-Th-Pb petrochronology, oxygen-isotopes, crustal flow

1. Introduction

In their core, most orogens consist of abundant quartzofeldspathic metamorphic rocks (gneiss, migmatite) that record low-pressure, high-temperature (L*P*-H*T*) conditions. Less abundant refractory rocks hosted in gneisses and migmatites, such as eclogites or granulites, record high-pressure (H*P*) metamorphism (e.g., Bodinier et al., 1988; Cabanis & Godard, 1987; Cuthbert et al., 2000; Eskola, 1921; Little et al., 2011; Möller et al., 2015; O'Brien, 2019; Štípská et al., 2008; Zheng et al., 2018). The origin of eclogites and their relationship to their felsic hosts has long been debated (e.g. Brueckner, 2018), with eclogites often interpreted as having a separate, asynchronous metamorphic history from the gneisses due to the apparent difference in peak *P*-*T* conditions recorded by the two lithologies. An additional challenge is the scarcity of geochronometers such as zircons in mafic protoliths (e.g. Shao et al., 2019), and the fact that zircons, even if present in the mafic rocks, do not systematically grow or recrystallize metamorphic rims associated with the eclogite-facies metamorphic event (e.g. Paquette et al., 2017). However, in some cases, eclogite and gneiss experienced the same metamorphic event (Baldwin et al., 2004; Whitney et al., 2015, 2020), and the difference in preserved metamorphic conditions resulted from differential reactivity owing to bulk compositional differences (e.g. Herwartz et al., 2011). There is growing recognition that lithologies with seemingly disparate records of metamorphic conditions in metamorphic terranes may have experienced the same history and differentially re-equilibrated (e.g. Arab et al., 2021; Ferrero et al., 2021). The occurrence of eclogite and H*P* granulite in migmatite terranes may be evidence that the exhumed material was deeply sourced and that the migmatite domes represent the exposed tips of extensive deep crustal flow systems (Whitney et al., 2020).

The large-magnitude exhumation of deep crust in domes can be reconstructed from the *P-T* history of H*P* relics such as orogenic eclogite (e.g., Groppo et al., 2015; Herwartz et al., 2011; O'Brien, 2019; Štípská et al., 2008). Significantly more challenging is determining the extent of lateral flow that may have occurred prior to dome formation, as this part of the record is obliterated in most exhumed rocks. One possible clue to investigate lateral flow of the deep crust is the extent to which zircon has (re)crystallized during metamorphism, a process likely facilitated by interaction with partially molten crust and/or fluids during deformation, or in response to prolonged time spent at elevated temperatures. The chemical and textural characteristics of zircon and coexisting phases such as garnet and rutile provide key information about the origin and history of eclogite, from protolith petrogenesis through metamorphic history.

In this study, we investigate the conditions, chemical environment, and timing of metamorphism of H*P* mafic rocks exhumed in three localities in the Montagne Noire migmatite dome, France. Previous studies of the Montagne Noire eclogites focused on fundamental characterization of *P-T-t* conditions in the context of dome formation. However, the protolith origin and timing of high-*P* metamorphism recorded by these eclogites is still debated in the literature, proposed as either oceanic crust subducted at *c.* 360 Ma, subsequently incorporated into H*T*-L*P* crust and recrystallized at low-*P* during doming (e.g. Faure et al., 2014; Pitra et al., 2021), or continental mafic material eclogitized at 315-310 Ma in the late stages of the Variscan orogeny as a result of crustal thickening (Whitney et al., 2015, 2020) shortly followed by exhumation with associated gneisses and migmatites. These hypotheses have significantly divergent implications for the magnitude of deep crust cycling during orogenesis, and yet a determination of the chemical environment – including fluid composition, trace and rare earth

element availability – of zircon formation and recrystallization in these eclogites has not been undertaken. In this study, we investigate the geochemical signature of individual zircon domains using, for the first time in eclogites from the French Massif Central, *in situ* U-Pb petrochronology of zircon and rutile by laser-ablation split-stream (LASS)-ICP-MS with compositional and oxygen-isotope analyses of garnet (*in situ*) and zircon by SIMS. The microgeochemical behavior of these minerals can be linked to the timing, conditions (*P*, *T*), and chemical environment (fluids/melt) in which they formed to investigate differences in the extent of zircon (re)crystallization and occurrence of prograde features in garnet in eclogites exhumed in different structural domains of the dome. Our results show that eclogite from the structural core and margin of the Montagne Noire preserves different records of protolith formation, prograde and/or H*P* metamorphism and fluid-rock interactions, although H*P* metamorphism was coeval in all analyzed eclogite. We document the origin, trajectory, and magnitude of flow of material incorporated and exhumed in a crustal flow system and propose a qualitative method for reconstructing the trajectories and evaluating the relative extent of deep-crust lateral flow in dome systems at the orogen scale.

2. Geologic setting

2.1 The Montagne Noire and the Massif Central

The Montagne Noire is a migmatite dome located at the southernmost margin of the Variscan French Massif Central (FMC), between foreland nappes (south) and a thrust system (north) (Fig 1). The metamorphic core of the Montagne Noire is primarily composed of paragneiss and orthogneiss and structurally consists of two main subdomes (Fig. 1). The subdomes are separated by a median high-strain zone characterized by steeply-dipping foliations (Rabin et al., 2015). The

Figure 1. Full-width page, Color

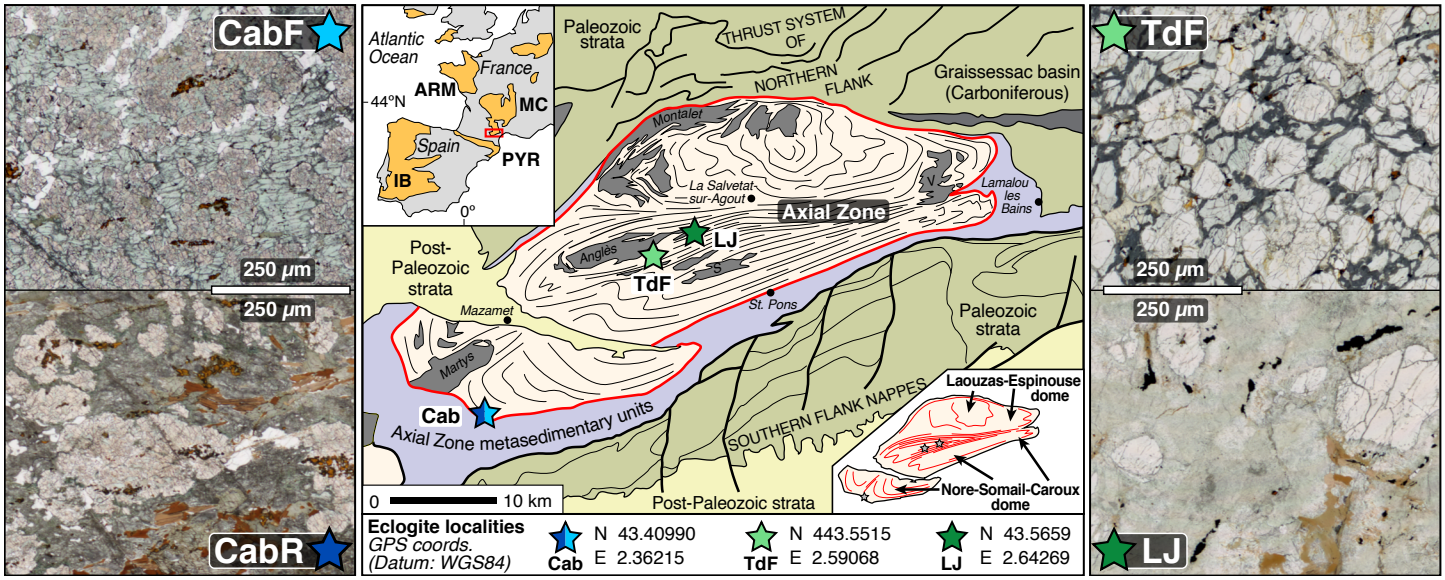

Figure 1. Simplified geologic map of the Montagne Noire (upper left inset: relationship to Variscan exposures in yellow: IB = Iberian, PYR = Pyrenees, ARM = Armorican, and MC = Massif Central) after Whitney et al. (2020) and references therein, showing the distribution of eclogite localities and samples used in this study. Schematic foliation trends in the Axial Zone of the Montagne Noire are represented by curved grey lines; anatectic granitic intrusions are represented in dark grey on the map (S = Soulié, V = Vialais). Eclogite samples are identified as follows – dome-core samples: TdF = Terme de Fourcaric, LJ = Le Jounié (green stars); dome-margin samples: Cab = Cabardès (blue star). Representative thin section images of all four eclogite samples are shown in the left (dome-margin) and right (dome-core) panels, with fresh eclogites TdF and CabF (F = Fresh) at top, and retrogressed eclogites LJ and CabR (R = Retrogressed) on the bottom. Lower right inset highlights main structural subdomains of the Axial zone in relationship to eclogite localities. GPS coordinated for all samples in this study: Whitney et al., (2020), Table 1.

gneissic core is separated from the thrust belts by a structurally-overlying metasedimentary carapace (Demange, 1994; Franke et al., 2011; Rabin et al., 2015). The carapace consists of schist and phyllite that contain L*P* index minerals such as andalusite and cordierite, and scarce relict kyanite (Bouchardon et al., 1979; Fréville et al., 2016) indicative of earlier higher-*P* metamorphism. Metamorphic grade of the schist decreases significantly from sillimanite zone near the gneissic core to slate-phyllite away from the dome (Doublier et al., 2014; Fréville et al., 2016; Thompson and Bard, 1982).

The Montagne Noire also contains crustally-derived granitic intrusions (e.g., Aerden, 1998; Bouchardon et al., 1979; Demange et al., 1996; Géze, 1949; Roger et al., 2015; Schuiling, 1960), lithologically heterogeneous and highly strained fine-grained gneiss (e.g. Roger et al., 2020), amphibolite layers, and mafic to ultramafic pods hosted by gneiss/migmatite (Demange, 1985; Faure et al., 2014; Whitney et al., 2015, 2020). Here, we focus on the volumetrically minor but petrologically significant eclogite pods.

2.2 Timing and P-T conditions of metamorphism in the Montagne Noire

High-*T* metamorphism, migmatization, and associated deformation of gneiss and schist in the dome core occurred at *c.* 315-300 Ma, as determined by U-Th-Pb dating (Franke et al., 2011; Poujol et al., 2017; Roger et al., 2015, 2020; Trap et al., 2017). Host gneiss magmatic protolith ages were dated at *c.* 550-520 Ma and 470-450 Ma (zircon and monazite U-Th-Pb) (Roger et al., 2020 and references therein), similar to ages determined for gneiss throughout the Massif Central and Pyrenées (e.g. Vanderhaeghe et al., 2020). Recorded peak-*T* conditions of ~730ºC at $P = 0.8 \pm 0.1$ GPa for the Caroux subdome, and 725 ± 25ºC at $P = 0.8 \pm 0.15$ GPa for the Espinouse

subdome, which also records retrograde conditions of P ~0.4 GPa, and T ~690-700ºC, are associated with partial melting of felsic lithologies in the migmatitic core (Fréville et al., 2016).

The timing of HP metamorphism recorded by eclogites in the Montagne Noire is still debated: Whitney et al. (2015, 2020) concluded that the HP event occurred at *c.* 315-310 Ma, based on LA-ICPMS U-Th-Pb dating and REE characterization of zircon rims in fresh eclogites from the core and margin of the dome, whereas Pitra et al. (2021) attributed these ages to recrystallization under LP-HT conditions, with flat HREE patterns explained by a proposed decoupling of the U-Pb and REE systems during recrystallization. Faure et al. (2014) also dated rutile and zircon from this retrogressed eclogite and obtained ages of 315–309 Ma, interpreted as the age of "hydrothermal" metamorphism. Whitney et al. (2015, 2020) further proposed that these ages indicate that eclogite facies metamorphism (315–310 Ma) was coeval with the beginning of migmatization (Roger et al., 2015, 2020; Trap et al., 2017). The meaning and tectonic significance of these ages is therefore debated. More detailed petrochronology data are needed to investigate the settings of protolith formation, processes taking place at eclogite-facies metamorphism, and explain the differences in zircon textures and extent of recrystallization between dome-core and dome-margin eclogites: this is the focus of our paper.

In these previous studies, conditions of HP metamorphism were determined for the eclogites using equilibrium thermodynamic modeling (Whitney et al., 2015, 2020; Pitra et al., 2021) and trace-element thermobarometry (Whitney et al., 2015, 2020), with slightly different results based on the solid solution models and approaches used to estimate effective bulk composition, H_2O and Fe^{3+}. Whitney et al. (2015, 2020) determined peak-P conditions of ~ 1.5 ± 0.2 GPa at T ~ 700 ± 20°C for fresh eclogites in the core (TdF) and margin (Cabardès, CabF) of the dome; these data were interpreted to indicate eclogitization in an orogenic setting driven by

crustal thickening at high-*T*. Pitra et al. (2021) calculated *P*-*T* conditions interpreted to represent a portion of the prograde path from ~1.95 GPa and ~700°C to a peak-*P* of ~2.1 GPa at 750°, which they deemed incompatible with crustal thickening and attributed to subduction.

3. Eclogite samples

Two localities with metabasaltic eclogite preserving garnet + omphacite are documented: *Terme de Fourcaric* (TdF) is located in the median high-strain zone of the dome-core, and *Cabardès* (Cab) near the dome-margin, close to the boundary between the dome gneiss and schist carapace (Fig. 1). Retrogressed eclogite also occurs at *Le Jounié* (LJ), ~5 km from the TdF locality in the dome-core (Fig. 1). Eclogites outcrop as boulderish bodies and are surrounded by quartzofeldspathic gneiss and migmatite (Whitney et al., 2015, 2020). We analyzed four eclogite samples: two fresh eclogites with omphacite + garnet (CabF, TdF), and two retrogressed eclogites containing garnet and either some relict (CabR) or no omphacite (LJ).

3.1 Dome-core eclogites

The TdF eclogite is equigranular and contains a peak assemblage of garnet + omphacite + rutile + quartz. Small (~2 mm) subhedral to rounded garnet contains quartz inclusion-rich cores, and largely clear rims with sparse rutile inclusions (Fig. 2a). Garnet also contains small, rounded zircon inclusions in both cores and rims. Rutile occurs in the matrix, as anhedral crystals commonly partially replaced by ilmenite (Fig. 2a).

The retrogressed dome-core eclogite (LJ) was overprinted in the amphibolite facies. It retains no omphacite but contains abundant symplectites of hornblende + plagioclase ± quartz (Smp_1, Fig. 2b) and large garnet porphyroblasts (up to 5 mm) partially replaced by symplectite

Figure 2. Full-width page, Color

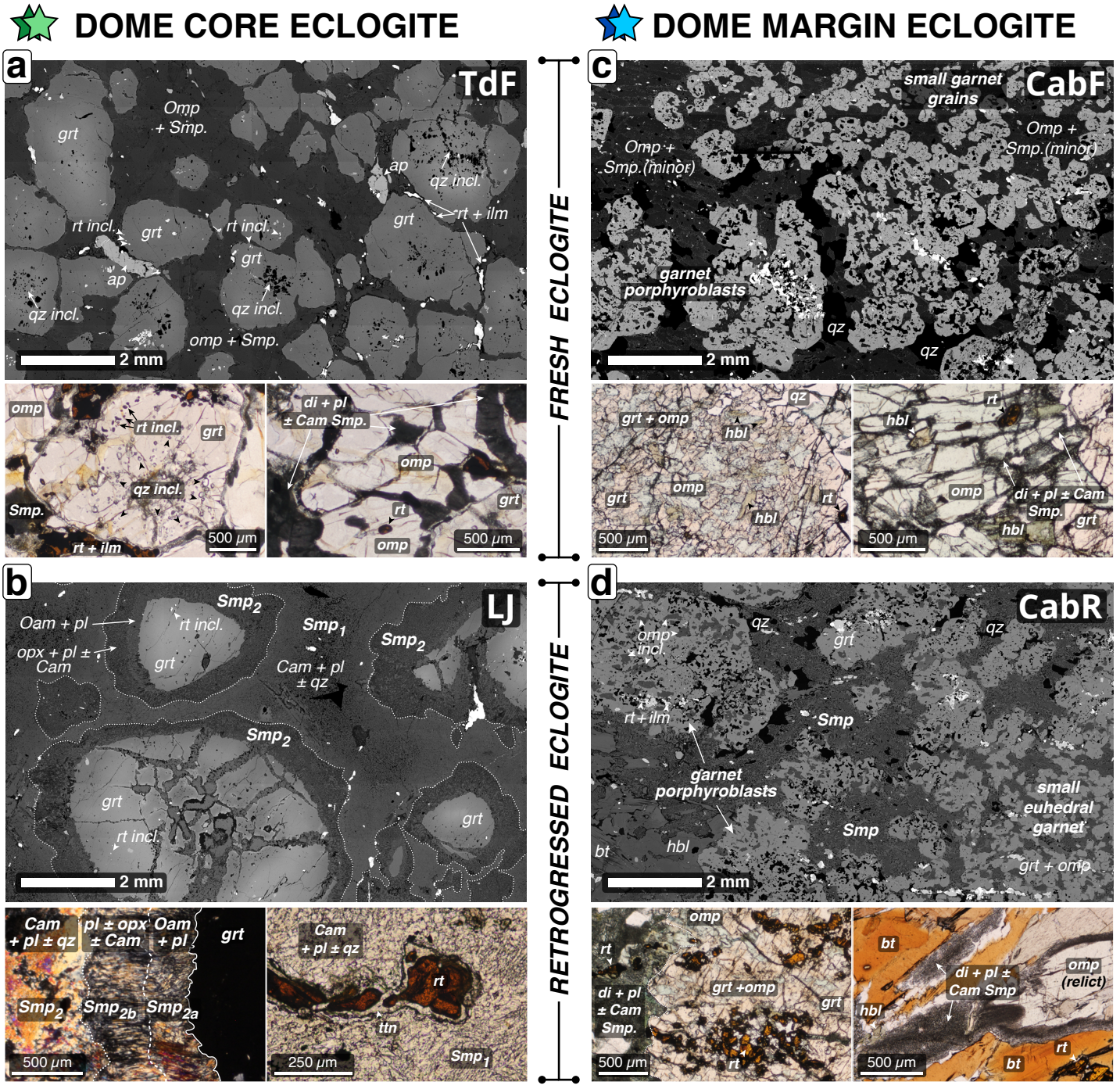

Figure 2. Representative textures of eclogites. Dome-core: a) top: backscatter electron (BSE) image of the TdF eclogite; left: plane-polarized light (PPL) image of subhedral garnet with quartz-inclusion-rich cores and inclusion-poor rutile-bearing rims; right: PPL image of matrix omphacite with extremely fine-grained (grey) symplectites after omphacite, rutile present in the matrix; b) BSE image of LJ retrogressed eclogite, dotted lines represent the original garnet-matrix boundary, matrix is entirely symplectite after omphacite (Smp1), garnet grains have undergone extensive partial replacement at the rim (Smp2); left: cross-polarized light (XPL) image of Smp1 and Smp2 symplectite domains. Smp2a and Smp2b represent different garnet replacement symplectite assemblages; right: PPL image of matrix rutile partially replaced by titanite at the rim and surrounded by fine-grained Smp1 phases. Dome-margin: c) BSE image of CabF eclogite highlighting bimodal garnet size distribution; left: PPL image of a large garnet grain with numerous inclusions of omphacite and few hornblende inclusions; right: PPL image of well-preserved matrix omphacite with limited symplectization at omphacite grain boundaries; rutile and hornblende present in the matrix; d) BSE image of CabR retrogressed eclogite; left: PPL image of a large garnet grain with abundant omphacite and rutile inclusions, similar to CabF but with extensive replacement of omphacite by symplectite in the matrix; right: PPL image of coarse-grained biotite and hornblende grains in the matrix, with relict omphacite partially replaced by fine-grained symplectite.

(Smp$_2$) of orthoamphibole + plagioclase and clinoamphibole + plagioclase ± orthopyroxene (Fig. 2b). Rutile occurs in the matrix, with local titanite replacement at the rims, and as inclusions in garnet.

3.2 Dome-margin eclogite

Two samples from the same eclogite block were analyzed. CabF (F: fresh) was sampled from the core of a boulder, whereas CabR (R: retrogressed) was sampled from the outermost part of the boulder and was more extensively overprinted at amphibolite facies. Cab samples contain two garnet populations: coarse-grained garnets up to 3 mm in diameter contain evenly distributed large omphacite, rutile, sparse green amphibole and rare quartz inclusions, whereas aggregates of smaller (<500 μm) subhedral to euhedral garnets are largely inclusion-free, although inclusions of quartz, omphacite, epidote, and rutile occur (Fig. 2c,d).

The matrix of CabF contains euhedral omphacite with minor symplectite at grain boundaries, and smaller grains of green amphibole and rutile. Symplectization of the matrix is advanced in CabR, with fine-grained symplectites of diopside + blue-green amphibole + plagioclase, and coarse-grained laths of biotite and green amphibole replacing the matrix symplectite. There is some relict omphacite in the CabR eclogite matrix, whereas omphacite inclusions in garnet are well-preserved and show little sign of alteration (Fig 2c.). Rutile occurs in the matrix and as inclusions throughout garnets in both Cab samples (Fig. 2c,d).

4. Analytical methods

4.1 Petrochronology (zircon, rutile)

U-Th-Pb petrochronology of zircon was primarily carried out to document the microchemical fingerprints (U-Pb dates, trace element and REE signatures) of individual zircon domains targeted for O-isotope analyses. U-Th-Pb data and REE compositions of zircon and rutile were analyzed by (LASS)-ICP-MS at the University of California – Santa Barbara on a Photon Machines Analyte 193nm Excimer Laser with HelEx ablation cell, combined with a Nu Instruments HR plasma high-resolution multi-collector ICP-MS (U-Th-Pb) and an Agilent 7700S quadrupole ICP-MS (REEs). Detailed analytical protocols are described in Kylander-Clark et al. (2013) and in supplement A1. Additional geochronology results for LJ eclogite zircon analyzed by SHRIMP-II (methods in Whitney et al., 2020) are in Supplement C.

4.2 SIMS oxygen-isotope analyses (garnet, zircon)

Oxygen-isotopes of garnet and zircon were analyzed by Secondary Ion Mass Spectroscopy (SIMS) at the University of Madison-Wisconsin WiscSIMS lab on a Cameca IMS-1280 following the procedure described in Kita et al., 2009 and Valley & Kita, 2009. Detailed SIMS analysis procedures are in supplement A2.

4.3 EPMA analyses

To provide context for oxygen isotope analyses of garnet and data for correction of compositional bias (Page et al., 2010), we measured major-element compositions by electron-probe microanalysis (EPMA) at the University of Minnesota on a JEOL-8550FPlus Electron Probe. Detailed EPMA methods are in supplement A3.

5. Results

We present zircon and rutile U-Pb petrochronology results (Table 1), and zircon and garnet O-isotope analysis (Table 2) from the four eclogites. The full zircon petrochronology dataset is in supplementary Table B (zircon, LASS-ICP-MS) and Table C (SHRIMP-II). Rutile LASS-ICP-MS data are in supplementary Table D. The full O-isotope dataset is in supplementary Table E and garnet compositions are in Table F. In the text and figures, all uncertainties in dates are given at ±2σ.

5.1 Zircon petrochronology

We identified two types of zircon textures (I, II). Type-I zircons have distinct CL-dark cores and CL-bright rims (CL: cathodoluminescence). Type-Ia zircons are characterized by CL-dark cores with small (<1 μm) rounded quartz inclusions from which fractures radiate in many of the grains (BSE, SE and CL images in Supplement A2); Type-Ib zircons are devoid of quartz inclusions, minimally fractured, and have very thin (<10 μm) CL-bright rims (e.g. gr#35,38 Fig. 3i, Figure B3). Type-II zircons have no inherited core and display intermediate-CL gray colors, with patchy zoning (e.g. gr#057, 049, Fig. 3a). Dome-core eclogites (TdF, LJ) contain only Type-Ia and Type-II zircons, and the TdF eclogite has the sparsest record of preserved CL-dark cores. Dome-margin eclogite (CabF, CabR) exclusively contains Type-Ib grains.

To detect potential differences in recorded dates, we classified zircon grains by their relationship with the overall rock texture: zircon grains in the matrix, at garnet-matrix boundaries, and as inclusions in garnet. For the retrogressed LJ eclogite, we separated zircons by their occurrence as inclusions in garnet or in symplectites replacing either omphacite (Smp_1) or garnet (Smp_2). Type-Ia grains occur in all three textural domains, whereas the majority of Type-

Table 1 - single column, Greyscale

Sample, phase	Age (Ma) ±2σ [1]	MSWD$_{C+E}$	n	$^{207}Pb/^{206}Pb_{init.}$	Th/U[2]	Eu*[2]	$[Lu/Dy]_N$[2]	n[3]	Log(Cr/Nb) [2]	Nb/Ta[2]	$T_{zr\text{-}in\text{-}rt}$ ± 2σ (°C)
DOME CORE											
TdF (MN13-11)											
Zrn (T-Ia cores)	434-400	NA	4	–	~ 0.3 *[n = 2]* ~ 1.9 *[n = 2]*	~ 0.1 *[n = 2]* ~ 1 *[n = 2]*	~ 1.5–3 *[n = 2]* ~ 0.5 *[n = 2]*	4	–	–	–
Zrn (T-Ia rims; T-II)	313.0 ±1.9	0.55	18	–	< 0.1	~1	~ 0.1 *[n = 9]* ~ 0.5–1 *[n = 4]*	13	–	–	–
Rutile	304.2 ± 5.7	2.1	45	0.76 ± 0.10	–	–	–	–	~ 0.5	~ 16	719 ± *30*
LJ (MN13-08)											
Zrn (T-Ia cores)	495-412	NA	7	–	~ 0.4–1.8	~ 0.2–0.3 *[n = 5]*	~ 0.2–0.6 *[n = 6]*	7	–	–	–
Zrn (T-Ia rims; T-II)	320.2 ± 2.8	1.2	9	–	< 0.1	~ 1	~ 0.1 *[n = 4]*	5	–	–	–
Rutile	307.3 ± 4.5	1.15	38	0.914 ± 0.18	–	–	–	–	~ 0.4	~ 16	715 ± 35
DOME MARGIN [4]											
CabR (MN16-05B)											
Zrn (T-Ib cores)	442.5 ± 3.4	1.7	17	–	< 0.8	~ 1	~ 0.7–1.4	20	–	–	–
Zrn (T-Ib rims)	*304 ± 9* [3]	NA	1	–	< 0.1	~ 0.6	< 0.1	1	–	–	–
Rutile	307.4 ± 2.9	1.17	47	0.846 ± 0.16	–	–	–	–	~ -0.3	~ 20	673 ± 30
CabF (MN16-05A)											
Rutile	322 ± 13	1.2	31	0.85 ± 0.03	–	–	–	–	~ -0.1	~ 23	678 ± 30

[1] Zircon: concordia age, or range of dates for groups of analyses where concordia age could not be calculated; rutile: lower intercept age.
[2] Th/U, Eu* and $[Lu/Dy]_N$ values represents the range of values excluding atypical values.
[2] typical values for Eu*, Lu/Dy and Th/U are given and brackets indicate # of spots associated with the representative value. These values are representative of analyses marked as '**R**' (rim) in the last column of table B, not exclusively from spots used for concordia age calculation (mixed analyses are not included for T-Ia rim/T-II analyses); due to the small amount of spots placed on core domains '**C**', for TdF and LJ cores, minorly mixed '**c**' (core-dominant component) analyses are included in the calculations.
[3] single-spot value from this study (sparse evidence for Variscan rims);
[4] For dome-margin zircon petrochronology, summarized data includes analyses from the combined CabF and CabR zircons (Cab).

Table 1. Summary of U-Pb petrochronology (LASS-ICP-MS) results. U-Pb petrochronology: averaged values are reported and marked in tables B (zircon) and table D (rutile).

Table 2 - single column, Greyscale

Samples	O-isotope analyses summary							
	Wtd. mean $\delta^{18}O$	**95% conf.**	**MSWD**	**p(χ^2)**	**Dispersion[(1)] ω + ω_{upper}/-ω_{lower}**	**Wtd. mean $\delta^{18}O$ ± 95% conf. of ω [(2)]**	**$\delta^{18}O$** *min – max*	**n**
DOME CORE								
TdF (MN13-11)								
Garnet (Grt2)	9.43	0.05	3.56	<< 0.01	0.17 +0.05/-0.04	9.43 ± 0.34	8.92 – 9.94	66
Garnet (Grt3)	9.59	0.03	1.26	0.032	0.09 +0.04/-0.04	9.59 ± 0.18	9.14 – 10.16	116
Garnet (all spots)	***9.52***	***0.03***	***2.34***	***<< 0.01***	***0.15 +0.03/-0.03***	***9.52 ± 0.30***	***8.92-10.16***	***182***
Zircon (Core, T-Ia) [(3)]	9.71	0.13[1]	*NA*	*NA*	*NA*	*NA*	*NA*	1
Zircon (mantle, T-Ia)	9.98	0.08	1.85	0.10	0.06 +0.14/-0.06	9.98 ± 0.12	9.39 – 10.19	6
Zircon (Rim, T-Ia)	10.02	0.08	1.67	0.11	0.06 +0.11/-0.06	10.02 ± 0.13	9.86 – 10.19	8
Zircon (T-II)	10.17	0.07	5.34	<< 0.01	0.18 +0.07/-0.05	10.17 ± 0.34	9.75 – 10.58	33
LJ (MN13-08)								
Garnet (Grt1)	8.60	0.08	0.93	0.51	NA	NA	8.41 – 8.80	12
Garnet (Grt2)	8.64	0.04	1.05	0.39	0.04 +0.07/-0.04	8.64 ± 0.07	8.39 – 9.05	44
Garnet (all spots)	***8.64***	***0.04***	***1.02***	***0.43***	***0.03 +0.07/-0.03***	***8.64 ± 0.05***	***8.39 – 9.05***	***56***
Zircon (Core, T-Ia)	8.76	0.06	1.72	0.088	0.04 +0.10/-0.04	8.76 ± 0.08	8.62 – 9.03	9
Zircon (mantle, T-Ia)	9.05	0.12	6.04	<< 0.01	0.18 +0.13/-0.07	9.05 ± 0.36	8.80 – 9.47	13
Zircon (Rim, T-Ia)	9.24	0.09	4.18	<< 0.01	0.14 +0.09/-0.06	9.24 ± 0.28	8.94 – 9.57	15
Zircon (T-II)	9.25	0.10	2.12	0.02 (< 0.05)	0.11 +0.12/-0.08	9.25 ± 0.21	9.03 – 9.47	11
DOME MARGIN								
CabF (MN16-05A)								
Garnet (Grt1)	8.06	0.04	1.49	<< 0.01	0.14 +0.04/-0.04	8.06 ± 0.28	7.57 – 8.45	80
Garnet (Grt3)	8.08	0.04	3.01	<< 0.01	0.14 +0.04/-0.03	8.08 ± 0.28	7.66 – 8.63	75
Garnet (Grt4)	8.03	0.04	1.06	0.34	0.08 +0.05/-0.06	8.03 ± 0.16	7.64 – 8.31	90
Garnet (all spots)	***8.06***	***0.02***	***2.31***	***<< 0.01***	***0.13 +0.02/-0.02***	***8.06 ± 0.26***	***7.57-8.94***	***245***
CabR (MN16-05B)								
Garnet (Grt2)	8.20	0.06	3.33	<< 0.01	0.12 +0.06/-0.05	8.20 ± 0.24	7.98 – 8.47	24
Garnet (Grt3)	8.21	0.05	1.12	0.29	0.06 +0.07/-0.06	8.21 ± 0.12	7.86 – 8.50	36
Garnet (all spots)	***8.20***	***0.04***	***1.96***	***<< 0.01***	***0.10 +0.04/-0.03***	***8.20 ± 0.20***	***7.86-8.50***	***60***
Zircon (Core, T-Ib)	8.24	0.11	3.75	<< 0.01	0.14 +0.11/-0.06	8.24 ± 0.27	7.98 – 8.57	11
Zircon (mixed, T-Ib)	8.34	0.10	1.04	*0.37*	*NA*	NA	8.22 – 8.49	4
Zircon (Rim, T-Ib)	8.49	0.20	9.07	<< 0.01	0.25 +0.24/-0.11	8.49 ± 0.49	8.10 – 8.83	7

[1] ω = st.dev of the true wt. mean $\delta^{18}O$ value after removal of the analytical uncertainties (model-3). $\omega > 0$ if p(χ^2) < 0.05 (95% uncertainty). Here, we also report ω for spot populations where p(χ^2) > 0.05 but dispersion is still present (slightly elevated MSWD > 1.05).
[2] NA values indicate non-dispersed subset of data
[3] Single-spot value, error given as analytical 2SD, not as 95% confidence; no range calculated.

Table 2. Summary of O-isotope data analysis (SIMS) results. Weighted mean $\delta^{18}O$ values for individual garnet grains and distinct zircon domains are given for all four eclogite samples analyzed, with the error reported at 95% confidence; for dispersed analytical groups, dispersion is reported and 95% conf. region of the dispersion (1.96×ω); One domain yielded a single validated spot analysis (TdF, zircon core, T-Ia), and the error for this spot is reported at '2SD' = analytical error from SIMS analyses, bracketed by KIM-5 zircon standard $\delta^{18}O$ value reproducibility. Full dataset can be found in Table E.

1 II grains occur in the matrix and near garnet-matrix boundaries. Overall, matrix zircon is larger
2 than zircon inclusions in garnet.
3
4 5.1.1 Zircon textures
5 TdF eclogite zircons are rounded to subhedral and 30-120 μm, with Type-II grains typically
6 larger than Type-Ia (Fig. 3a), with T-Ia and T-II zircons occurring in all textural domains
7 (inclusions in garnet and matrix). LJ retrogressed eclogite zircons are similar to those in the TdF
8 eclogite, but LJ Type-Ia zircons are slightly smaller (10-80 μm, Fig. 3e). Only two Type-II
9 grains were identified, both in symplectite domains. Type-Ia grains occur in all domains. Smp_1
10 zircons are large (10-80 μm) compared to Smp_2 zircons (15-60 μm), with the smallest grains
11 occurring as inclusions in garnet (5-50 μm) including small zircon aggregates characterized by
12 Type-Ia textures (gr#062, Fig. 3e). We were not able to analyze individual (core vs. rim)
13 domains in these small zircons, although we note that the CL-bright rims of zircon in these
14 aggregates are <1μm wide, resulting in the ablated volumes sampling predominantly CL-dark
15 cores of the grains.
16 CabF and CabR zircons are comparable in size, shape, and CL textures, so we combined
17 all analyses from the same session and refer to the sample as *Cab* in this section. Cab zircons are
18 rounded to anhedral, measure 5-60 μm (average ~40 μm) – smaller than dome-core eclogite
19 zircons (Fig. 3i). Internal textures of CL-dark cores include sector and/or patchy zoning
20 (gr#zrn02, 121, Fig. 3i), or intermediate CL-grey core surrounded by a CL-darker mantle, both
21 crosscut by the CL-bright rim domains (gr#030, Fig 3i). All CL-dark cores are surrounded by
22 thin CL-bright rims 1-15μm wide. The dominant texture is CL-dark core domains replaced at the

rim by irregular boundaries and embayment of CL-bright domains cross-cutting internal textures of the cores. Zircons are identical regardless of their textural associations.

5.1.2 Terme de Fourcaric fresh eclogite (dome-core)

The TdF eclogite yielded dominantly concordant zircon analyses defining a Variscan U-Pb zircon concordia age of 313.0 ± 1.9 Ma (Fig. 3b,c) obtained from CL-bright rims of Type-Ia and Type-II zircons, which are characterized by relatively flat HREE profiles with low Lu_N/Dy_N values ($Lu_N/Dy_{N\ avg}$ = 0.31 (n = 13), Fig 3d), no negative Eu anomalies (Eu^*_{avg} = 1.12), and low Th/U values (majority of Th/U << 0.1, Fig. 4a).

The four oldest dates are from mainly discordant analyses with ^{207}Pb-corrected $^{238}U/^{206}Pb$ dates between 434-400 Ma obtained on CL-dark cores and spots overlapping slightly with CL-bright domains (Table B). These four analyses are characterized by steeper HREE profiles ($Lu_N/Dy_{N\ avg}$ = 1.01 (n = 4), Fig. 3d) with negative Eu anomalies (Eu^*_{avg} = 0.71) and higher Th/U values (Th/U_{avg} > 0.2, Fig. 4a).

5.1.3 Le Jounié retrogressed eclogite (dome-core)

The LJ retrogressed eclogite yielded overall concordant zircon analyses scattered along concordia, between ~500–300 Ma in two age groups (see Table B). The first group yielded a Carboniferous (Variscan) concordia age of 320.2 ± 2.8 Ma (Fig. 3f,g) from Type-Ia zircon rims and Type-II zircons, characterized by low HREE enrichment (HREE/chondrite ~10^1) and flat HREE profiles ($Lu_N/Dy_{N\ avg}$ = 0.25 (n = 5), Fig 3h), lack of Eu-anomaly (Eu^*_{avg} = 0.99), and low Th/U values (Th/ << 0.1; Fig. 4a). The second group consists of spots yielding older dates scattered between 495–412 Ma (Fig. 3f, g) associated with Type-Ia zircon cores. Data scatter

Figure 3. Full-width page, Color

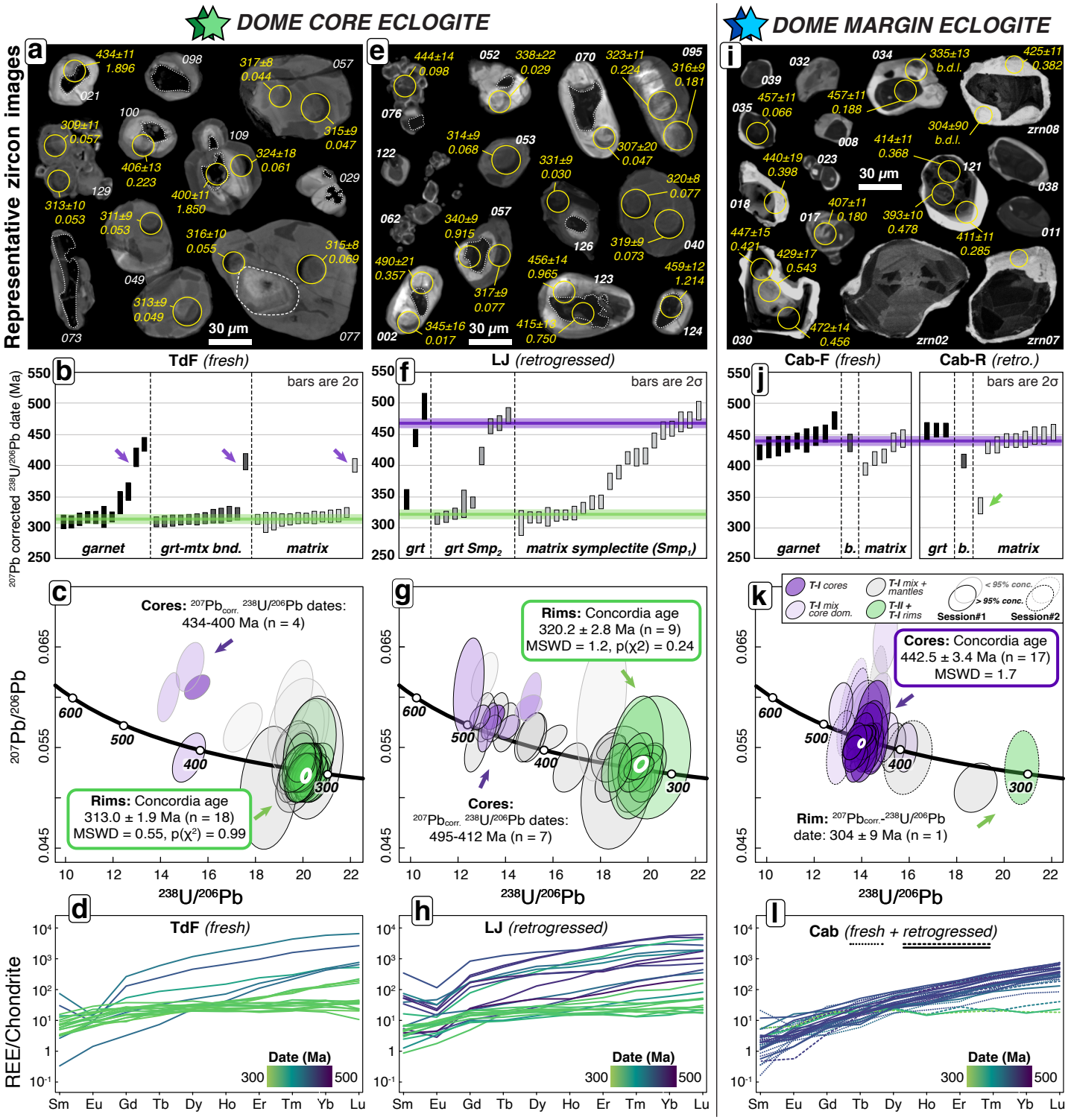

Figure 3. Zircon U-Pb petrochronology. Dome-core – TdF: (a)-(d), LJ: (e)-(h); Dome-margin – Cab: (i)-(l). a,e,i): CL-images of representative zircons, analytical spots with associated U-Pb dates and Th/U values for TdF, LJ, and Cab eclogites respectively, b,f,j) distribution of ^{207}Pb-corrected ^{238}U/^{206}Pb dates separated by textural association of analyzed zircons in TdF, LJ, and Cab eclogites respectively; c,g,k) Tera-Wasserburg plots of TdF zircon analyses and calculated concordia ages for zircon-rim and zircon-core analyses, where applicable, for TdF, LJ, and Cab eclogites respectively; MSDW given as MSWD of concordance + equivalence. Ellipses drawn are not corrected for common-Pb; however, for discordant or isolated analyses, ^{238}U/^{206}Pb date ranges are given after common-Pb correction on individual spots using the ^{207}Pb method (see Table B). Arrows indicate the location of zircon rim (green) and core (purple) analyses associated with corresponding date ranges or calculated concordia ages (boxed); d) chondrite-normalized REE plots of individual spot analyses color-coded by 2^{07}Pb-corrected ^{238}U/^{206}Pb dates for in TdF, LJ, and Cab eclogites respectively (plotted patterns indicated in Table B).

Figure 4. Half-width page, Color

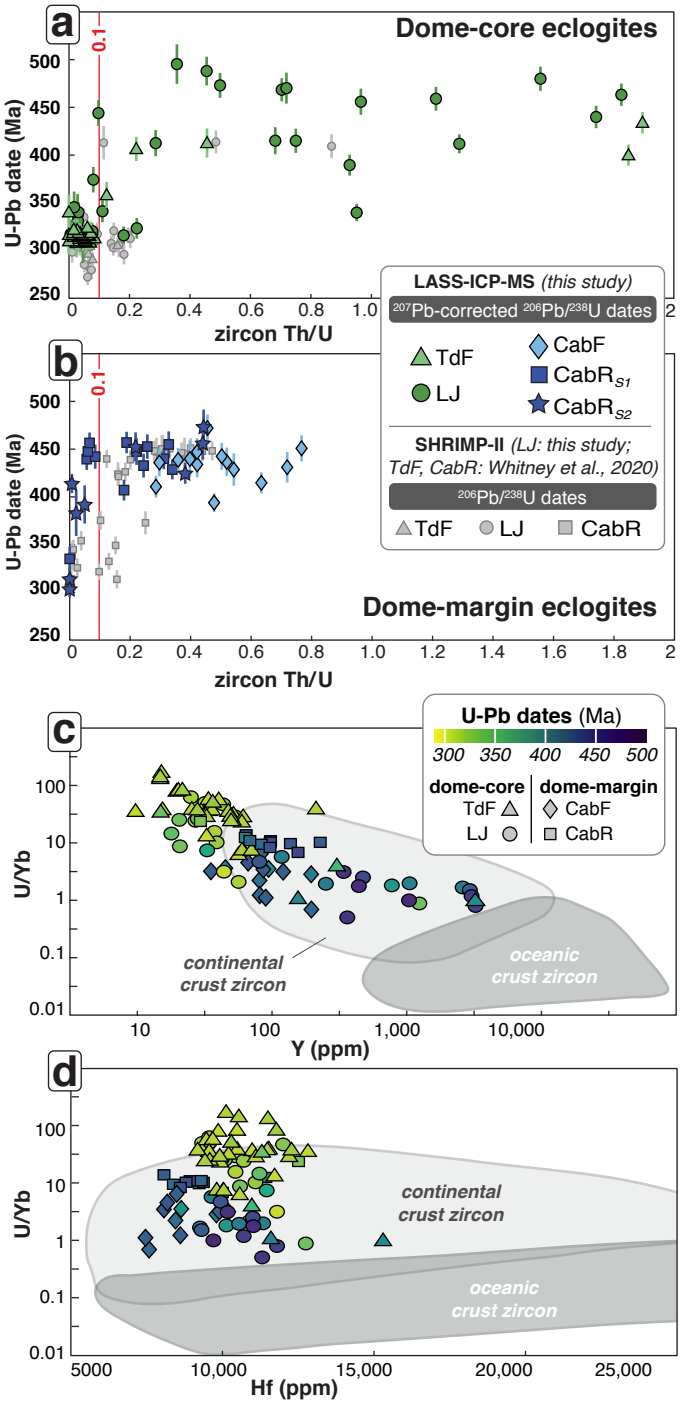

Figure 4. Zircon trace-element compositions. a) Th/U vs. U-Pb dates for dome-core eclogite zircons, vertical line at Th/U = 0.1 represents value commonly used to distinguish metamorphic (low Th/U < 0.1) from igneous (high Th/U > 0.1) zircon fields, along with U-Pb ages and REE patterns (Rubatto, 2002); b) dome-margin eclogite zircons; c) Y (ppm) vs. U/Yb and, d) Hf (ppm) vs. U/Yb plots of all LASS-ICP-MS zircon analyses, with individual spot analyses color-coded by ^{207}Pb-corrected ^{238}U/^{206}Pb dates. Continental and oceanic crust zircon fields from Grimes et al. (2007).

likely results from slight Pb-loss or minor mixing due to the analytical spatial resolution limit (~15 μm), small size (<30μm) and irregular shape of CL-dark cores, which exhibit CL-brightness variations and patchiness, or variable resetting, in which case the oldest date obtained would correspond to a minimum age for protolith crystallization. Analyses from LJ CL-dark cores are characterized by higher overall HREE enrichment (HREE/chondrite ~10^2-10^4), moderately steep HREE profiles ($Lu_N/Dy_{N\ avg}$ = 0.52 (n = 7), Fig. 3h), negative Eu-anomaly (Eu^*_{avg} = 0.31), and moderate to high Th/U values (Th/U from 0.4-2, Fig. 4a).

Moreover, U-Pb dating of LJ zircon by SHRIMP yielded 3 (out of 42 spots) older $^{238}U/^{206}Pb$ dates of ~410 Ma from CL-dark cores and mixed domains, with the remaining 32 spots placed on rims (1 spot discarded, high f_{206}%, Table C) yielding a continuous set of individual $^{206}Pb/^{238}U$ dates between 296-322 Ma (Fig. C), with a weighted mean average $^{206}Pb/^{238}U$ age of 310.3 ± 2.8 Ma and MSWD of 1.97 resulting from excessive dispersion.

5.1.4 Cabardès fresh and retrogressed eclogite (dome-margin)

The Cab eclogite yielded mostly concordant zircon analyses clustering around an Ordovician concordia age of 442.5 ± 3.4 Ma (Fig. 3j,k, spots from session 1 only) obtained exclusively from cores, and characterized by steep HREE profiles ($Lu_N/Dy_{N\ avg}$ = 1.04 (n = 20) Fig 3l), no Eu-anomaly (Eu^*_{avg} = 0.98, Fig. 3l), with mainly Th/U ratios > 0.1 and up to 0.8 (Fig. 4b).

Sparse evidence for Variscan dates from CL-bright rims is present due to the LASS-ICP-MS analytical spatial resolution relative to the rim size. The 440-300 Ma dates are probably mixed analyses biased towards zircon cores with higher U. One spot that exclusively sampled a zircon rim yielded a date of 304 ± 9 Ma, with Eu* = 0.62, Lu_N/Dy_N = 0.09 and Th/U~ 0 (Th

b.d.l.) (Table B), in accordance with results from Whitney et al. (2020), who dated the CL-bright zircon rims of the Cab eclogite at ~310 Ma, accompanied by Th/U values and a flat HREE slope.

5.1.5 Zircon U, Yb, Y, Hf trace-element compositions

Analytical spots yielding dates >400 Ma in all four analyzed samples plot in the 'continental zircon' field in U/Yb vs. Hf and U/Yb vs. Y plots (Fig. 4c, d), with U/Yb > 2, Hf > 13,000 ppm and Y < 3000 ppm. Younger dates are associated with elevated U/Yb values > 10 and Y < 100 ppm.

5.2 Rutile petrochronology

Dome-core eclogite rutile yielded lower intercepts of 304.2 ± 5.7 Ma (TdF) and 307.3 ± 4.5 Ma (LJ) (Fig. 5a,b), overlapping dome-margin eclogite rutile that yielded lower intercepts of 322 ± 13 Ma (CabF) and 307.4 ± 2.9 Ma (CabR) (Fig. 5c,d). The discordant position of the data in TdF, LJ and CabR is due to common Pb contamination only, with the data fitting a single regression line for each sample. We note the greater scatter in the rutile U-Pb data for the CabF eclogite, with some analyses falling on either side of the fitted regression line, indicating that the discordance for CabF is likely due to the combined effects of common-Pb contamination and Pb-loss, and may also be a mixture between Ordovician and Variscan components. Combined with very low U content (~1 ppm vs. 2-7 ppm in other samples), this explains the lower quality of the dates obtained, and we therefore do not attempt to interpret the significance of this scatter. For all four samples, we observe no correlation between dates (older vs younger) and textural setting of rutile (in the matrix vs. as inclusions in garnet). Rutile dates are consistent with zircon CL-bright

Figure 5. Full-width page, Color

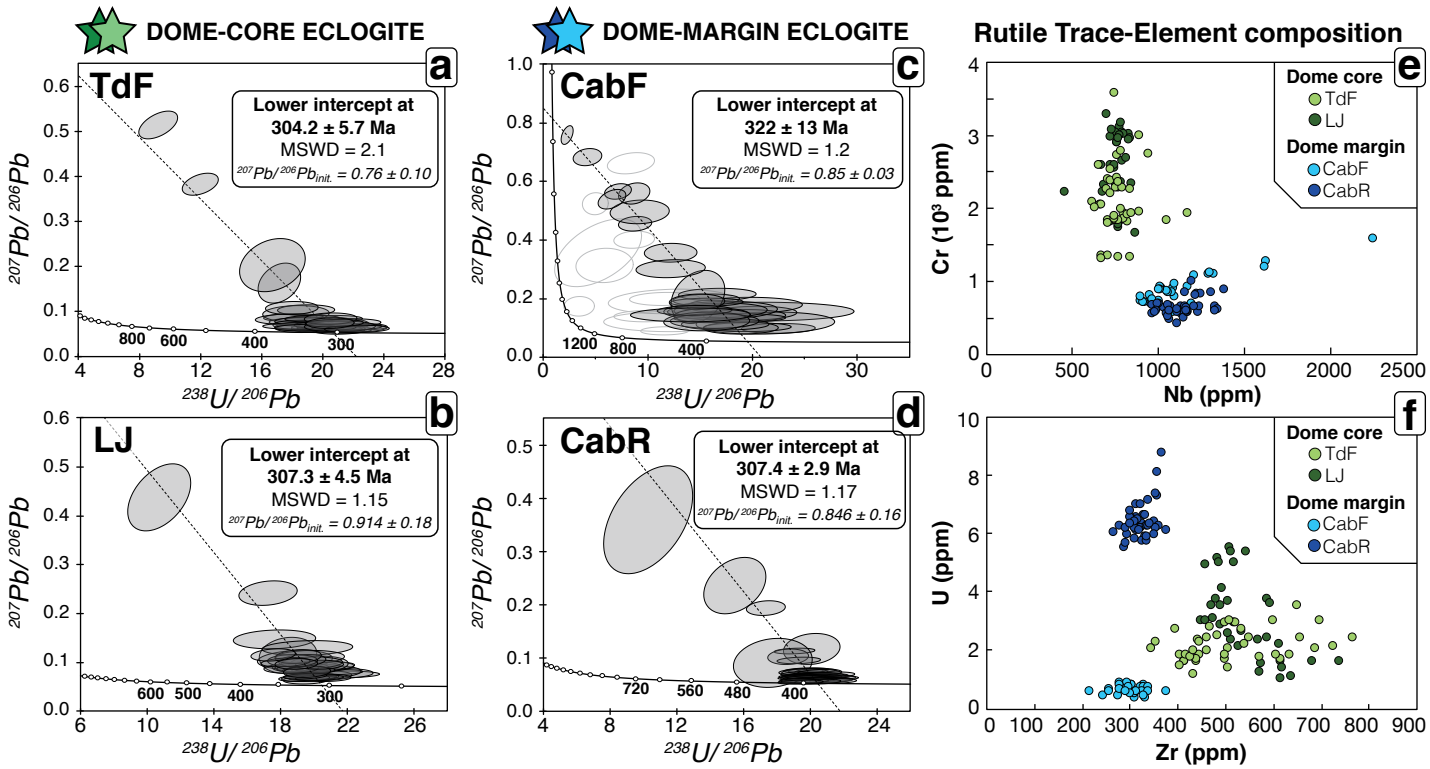

Figure 5. Rutile U-Pb petrochronology and trace-element compositions. Rutile Tera-Wasserburg plots for a) TdF, b) LJ, c) CabF, and d) CabR eclogites, with lower-intercept ages and y-intercept values calculated indicated for each sample. Rutile trace-element compositions: e) Nb (ppm) vs. Cr (ppm) and f) Zr (ppm) vs. U (ppm) plots showing distinct grouping of rutile compositions for dome-core vs. dome-margin eclogites.

rim dates reported here, by Whitney et al. (2015, 2020) for the TdF and Cab eclogites, and by Faure et al. (2014) for a retrogressed dome-core eclogite.

Rutile trace elements differ between the two structural domains of the dome. Dome-margin eclogite rutile is low in Cr (<1250 ppm) and high in Nb (>800 pm), whereas dome-core eclogite rutile is high in Cr (>1250 ppm) and low in Nb (<1000 ppm, Fig. 5e). Zr is less abundant in dome-margin rutile (<400 ppm) compared to dome-core rutile (> 400 ppm, Fig. 5f), consistent with the relatively higher temperatures recorded by dome-core eclogite (Whitney et al., 2020).

Given that zircon, rutile, and quartz occur in all textural domains and the lack of geochemical differences between rutile grains in different textural settings of the rock (i.e. inclusions in garnet vs. matrix rutile), we applied Zr-in-rutile (Tomkins et al, 2007 calibration, using P = 1.5 GPa) for the range of measured trace element concentrations. Mean $T(^{o}C)_{Zr\text{-}in\text{-}rutile}$ of 719 ± 30 ºC (TdF, n = 43) and 715 ± 35ºC (LJ, n = 38) for the dome-core and 673 ± 30ºC (CabR, n = 49) and 678 ± 30ºC (CabF, n = 42) for the dome-margin (Table D) are consistent with the temperatures of ~725°C and ~680ºC at peak-*P* reported by Whitney et al. (2015, 2020) for the dome-core and dome-margin, respectively, with dome-core temperature higher than dome-margin temperatures.

5.3 O-isotopes

5.3.1 Zircon

We analyzed core and rim domains of Type-Ia zircons (dome-core: TdF, LJ), Type-Ib (dome-margin: CabR) and Type-II zircons (TdF, LJ) to measure $\delta^{18}O$ values associated with different

U-Pb ages, REE and trace-element signatures (Fig. 6; Tables 1 and 2). All $\delta^{18}O_{wtd.avg}$ values are reported as weighted mean average (wtd.avg) at the 95% confidence level, which includes dispersion accounted for using a random effects model (see supplement A2).

5.3.1.1 Dome-core eclogite

We analyzed 6 Type-Ia grains and 13 Type-II grains from the TdF eclogite (Fig. 6a). Only 1 spot was obtained on CL-dark cores because many such grains had core domains that were too small or contained inclusions and cracks (Table E2). This spot yielded $\delta^{18}O$ values of 9.7 ±0.1‰, slightly lower than those of CL-bright rims, which yielded relatively consistent values with a $\delta^{18}O_{wtd.avg}$ of 10.0 ± 0.1‰ (8 spots). The single zircon spot analysis does not allow rigorous characterization of zircon core $\delta^{18}O$ in the TdF eclogite. Intermediate mantles between CL-dark cores and outer rims of Type-Ia zircon yielded a $\delta^{18}O_{wtd.avg}$ of 10.0 ± 0.1‰ (6 spots), identical to the rims. Type-II zircons yielded a $\delta^{18}O_{wtd.avg}$ of 10.2 ± 0.3‰ (33 spots) identical within uncertainty to Type-Ia zircon rims and mantles (Fig. 6a).

We analyzed 12 Type-Ia and 6 Type-II grains from the LJ retrogressed eclogite (Fig. 6b). Type-Ia zircon CL-dark cores yielded a $\delta^{18}O_{wtd.avg}$ of 8.8 ± 0.1 ‰ (9 spots). Type-Ia zircon rims yielded a $\delta^{18}O_{wtd.avg}$ 9.2 ± 0.3 ‰ (15 spots). For most grains, and spot placed within a single grain, the rims of individual zircons have higher $\delta^{18}O$ values than their cores within 2SD uncertainty. Type-II zircon yielded a $\delta^{18}O_{wtd.avg}$ of 9.3 ± 0.2‰ (11 spots), indistinguishable from Type-Ia rims.

5.3.1.2 Dome-margin eclogite

Figure 6. Full-width page, Color

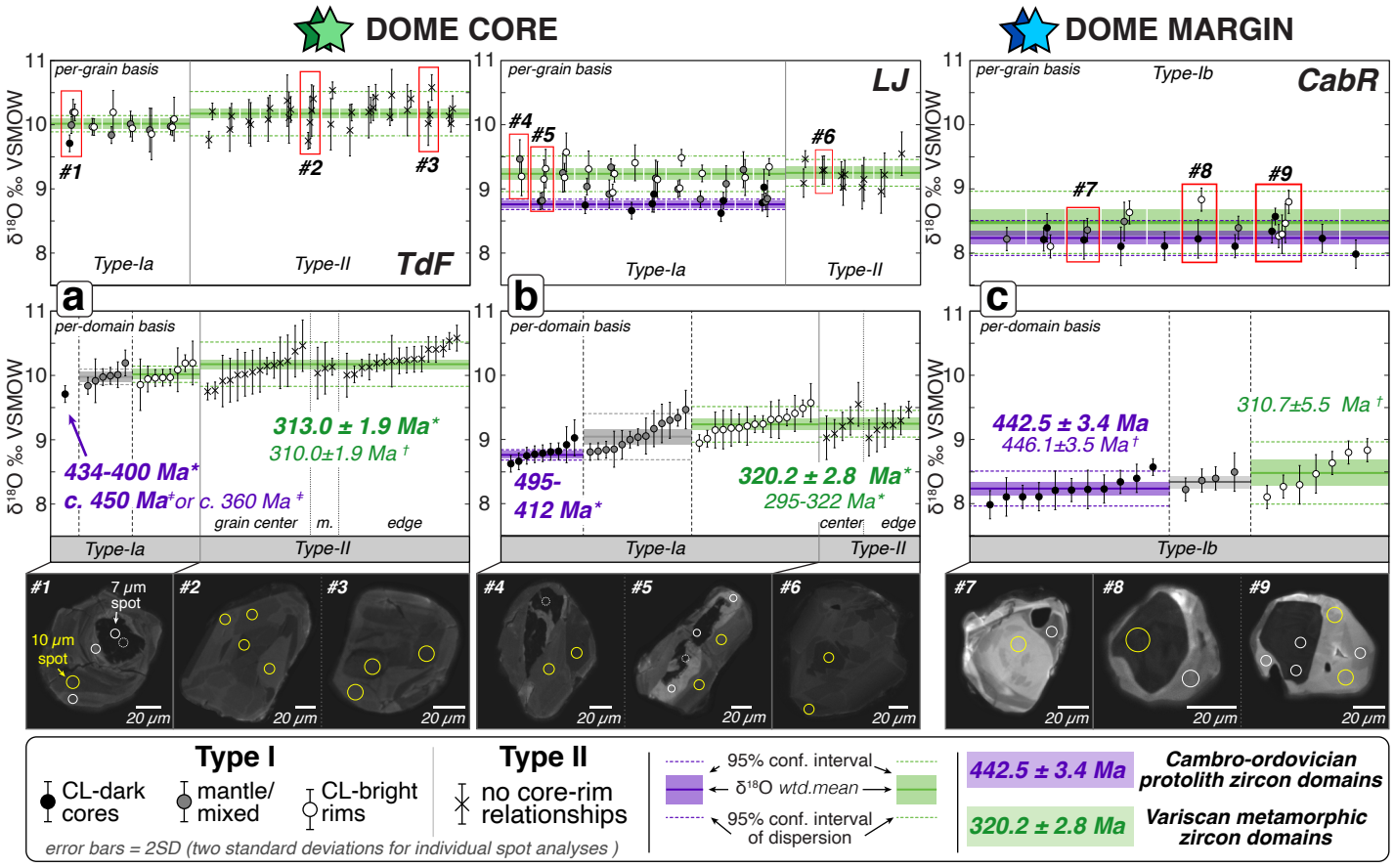

Figure 6. Zircon O-isotopes. Measured $\delta^{18}O$ values and associated 2SD error for individual spot analyses in a) TdF, b LJ and c) CabR eclogites. Top row: analyses plotted as 'per-grain basis' (white line between groups of analyses separates different grains analyzed); Middle row: compounded analyses plotted as 'per-domain basis' (T-I zircons: core, mantle, rim; T-II zircons: center, edge of grains); Bottom row: CL-images of representative Type-I and Type-II grains of TdF (a), LJ (b) and CabR (c) eclogites. U-Pb ages from this study and from the literature are indicated for zircon core (purple) and rim (green) domains. U-Pb ages: (*) this study, (≠)Whitney et al. (2015), (†)Whitney et al. (2020).

We analyzed 10 zircon grains from the dome-margin eclogite (CabR, Fig. 6c). CL-dark cores yielded a $\delta^{18}O_{wtd.avg}$ of 8.2 ± 0.3‰ (11 spots) and CL-bright rims yielded a similar average $\delta^{18}O_{wtd.avg}$ of 8.5 ± 0.5‰ (7 spots) within error. Four spots either resulted in mixed textural-domain analysis or were placed on ambiguous CL-textures (e.g. Fig. 6c, gr#7).

5.3.2 Garnet

We analyzed 2-3 garnets in each eclogite sample (Table 1, Table E2, Table F).

5.3.2.1 Dome-core eclogite

Garnet in the fresh (TdF) and retrogressed (LJ) dome-core eclogites is zoned in Ca (grs)-Fe (alm)-Mg (prp)-Mn (sps), with the following composition range: 34.0_{rim}-44.1_{core}% alm, 0.0_{rim}-1.9_{core}% sps, 34.4_{core}-49.1_{rim}% prp, 13.5_{rim}-23.7_{core}% grs (Fig. 7a). Garnet displays typical prograde growth zoning with Fe-richer core domains and Mg-richer, Fe-poorer rims. The two analyzed garnets in the TdF eclogite yielded the highest $\delta^{18}O$ values of all the analyzed samples, with $\delta^{18}O_{wtd.avg}$ values of 9.4 ± 0.3‰ and 9.6 ± 0.2‰ for TdF-grt#2 and garnet TdF-grt#3, respectively (Fig. 7b), with no significant $\delta^{18}O$ zoning from core to rim or differences in garnet cation zoning.

Garnet in the LJ sample is also zoned in major elements, with the following compositional range: 35.3_{rim}-58.1_{core}% alm, 0.0_{rim}-5.1_{core}% sps, 19.8_{core}-49.7_{rim}% prp, 10.3_{rim}-24.7_{core}% grs (Fig 7c). Like the TdF eclogite, large garnets are characterized by high-Fe, -Ca cores and high-Mg rims. Despite evident breakdown of garnet rims and replacement by symplectite, where preserved, the pyrope content of the rims is comparable to that of the rims of

Figure 7. Full-width page, Color

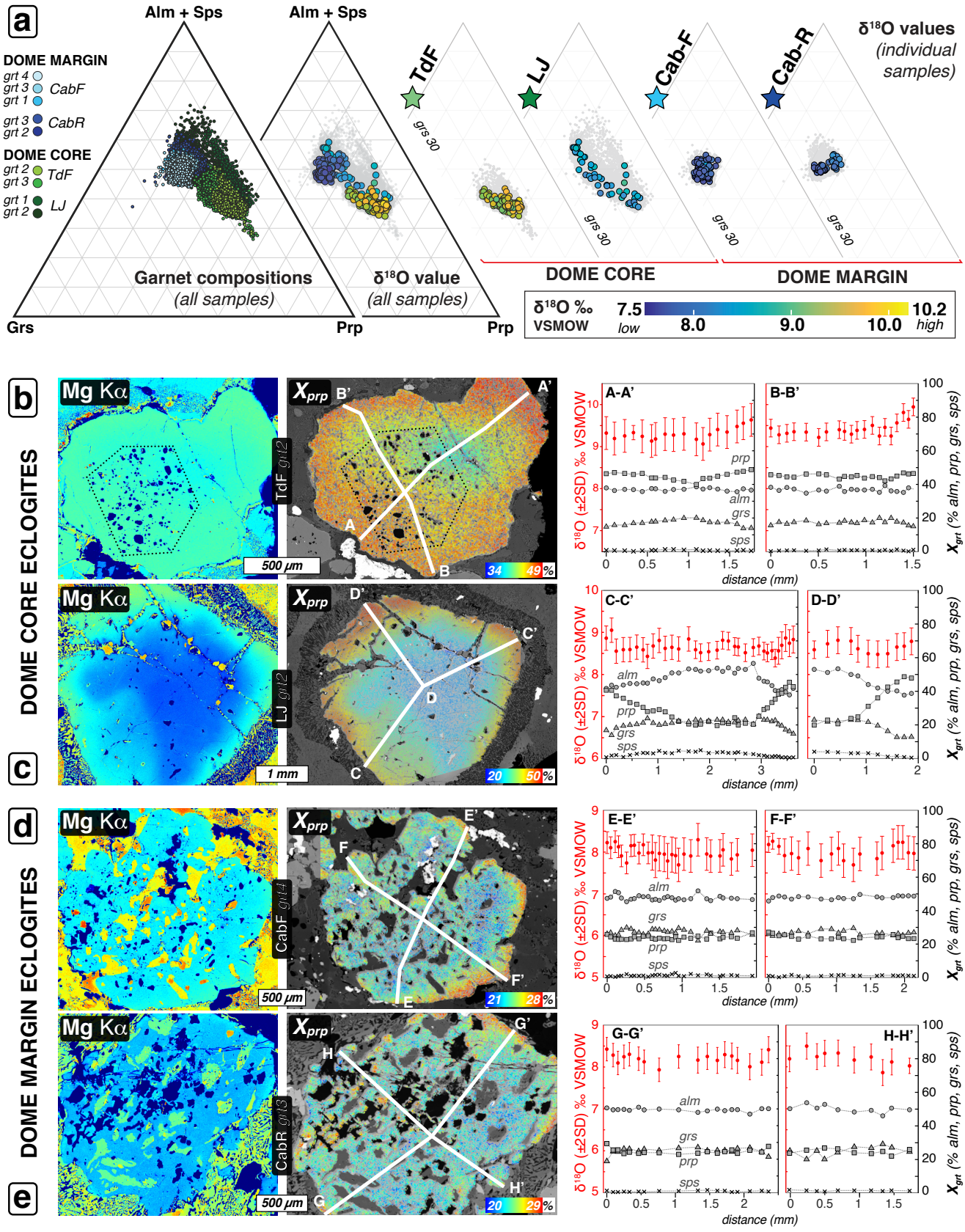

Figure 7. Garnet O-isotope and major-element compositions. a) ternary garnet composition plots for each sample and analyzed garnet (color coded by sample: green = dome-core, blue = dome-margin), garnet compositions with measured $\delta^{18}O$ values in garnet composition space, and ternary plots showing the range of $\delta^{18}O$ values for individual samples; (b)-(e) Mg-Kα EPMA map (left), calculated quantitative pyrope map overlain on BSE image (center), and $\delta^{18}O$ traverses and associated garnet end-member compositions of texturally representative garnets (right) in the a) TdF, b) LJ, c) CabF, and d) CabR eclogites. In garnet pyrope maps (center), the color gradient represents the range in pyrope compositions within each garnet and the range of values represented is given on the color bars in each image.

TdF garnet. LJ garnet has $\delta^{18}O_{wtd.avg}$ values of 8.6 ± 0.1‰ and 8.6 ± 0.1‰ for garnet LJ-grt#1 and garnet LJ-grt#2, respectively with no core-rim $\delta^{18}O$ zoning (Fig. 7c).

5.3.2.2 Dome-margin eclogite

Garnet in the dome-margin eclogites is not significantly zoned in Ca-Fe-Mg-Mn (Fig. 7d,e) nor is it systematically or significantly zoned in $\delta^{18}O$. CabF garnet compositions are as follows: 48.0% alm_{avg} (alm_{range}: 44.5-51.8%), 1.2 % sps_{avg} (sps_{range}: 0.2-2.3%), 24.3% prp_{avg} (prp_{range}: 20.9-27.9%), 26.5% grs_{avg} (grs_{range}: 22.7-30.2%). The three analyzed garnets from the CabF sample all have consistent $\delta^{18}O_{wtd.avg}$ values of 8.1 ± 0.3‰ (CabF-grt#1 grt#3) and 8.0 ± 0.2‰ (CabR-grt#4).

CabR garnet has slightly more compositional variability: 50.7% alm_{avg} (alm_{range}: 46.6-55.5%), 1.3% sps_{avg} (sps_{range}: 0.3-2.3%), 24.9% prp_{avg} (prp_{range}: 20.4-29.4%), 25.7% grs_{avg} (grs_{range}: 18.7-28.7%), similar $\delta^{18}O_{wtd.avg}$ values of 8.2 ± 0.2‰ and 8.2 ± 0.1‰ for CabR-grt#2 and CabR-grt#3 respectively. Small compositional variations in O-isotopes with lower $\delta^{18}O$ values associated with more grossular-rich regions are not correlated with core-rim zoning. Despite small differences in absolute value, CabF and CabR eclogites have overall consistent oxygen-isotope and major element compositions with little to no zoning in either system.

5.4 Summary of analytical results

Dome-margin eclogite zircon records two episodes of growth: at 442.5 ± 3.4 Ma (cores, enriched HREEs, no Eu-anomaly, moderate Th/U > 0.1 and up to 0.9), and at *c.* 315-310 Ma (rims, flat HREEs, Th/U << 0.1) (Table 1), for which we see only sparse evidence and are better constrained by Whitney et al. (2020). Zircon cores, rims, and isotopically and chemically

unzoned garnets have overlapping $\delta^{18}O_{wtd.avg}$ values of ~8.3‰ (Table 2). Dome-margin zircon rims are minimally recrystallized and occur both in the matrix and as inclusions in garnet.

Dome-core eclogite zircon also records two episodes of growth: Ordovician inherited cores (enriched HREEs, marked negative Eu-anomaly, Th/U > 0.2) have lower $\delta^{18}O$ (LJ: ~8.8‰; TdF: single spot analysis ~9.7‰) than rims and Type-II zircons dated at *c.* 320-310 Ma (LJ: ~9.3‰; TdF: ~10.1‰). And $\delta^{18}O$ zircon rim values are ~0.5‰ higher than garnet values (LJ: ~8.6‰; TdF: ~9.5‰); these garnets are zoned in Fe-Mg-Mn-Ca but unzoned in $\delta^{18}O$. Variscan zircon dates have flat HREE slopes, positive Eu-anomalies, Th/U <0.1.

Dome-core eclogite zircons are significantly larger and have more extensively recrystallized rims than dome-margin zircons, with TdF zircons being the most extensively recrystallized. Dome-core and dome-margin rutiles record a U-Pb dates of 307-304 Ma consistent with Variscan metamorphic zircon rims but have distinct trace-element compositions. Rutile in the matrix of retrogressed eclogite (CabR, LJ) is not in equilibrium with the dominant amphibolite-facies assemblage and is interpreted as a relic of the H*P* paragenesis.

6. Protolith to eclogite-facies history and implications for crustal flow systems

These results allow us to discuss the protolith to H*P* history of the Montagne Noire eclogites. We focus on possible processes responsible for differences in zircon textures and extent of recrystallization and discuss their implications for protolith source (distal vs. proximal), origin (magmatic processes), and conditions of metamorphism up to and at eclogite facies. We also discuss implications for time and length scales, as well as trajectories of material transport in the deep crustal flow system of the Variscan orogen.

6.1 Protolith source and origin

The CL-dark cores of zircons are textural and chemical relics of the eclogite protoliths. U-Pb dating of these scarce zircon cores in the dome-core yielded dispersed dates between 500–400 Ma compared to the well-constrained 442.5 ± 3.4 Ma age of the dome-margin eclogite zircons. These ages are consistent with those of the augen gneiss protolith that hosts the eclogite pods, dated at 470-450 Ma (e.g. Roger et al., 2004; 2020), supporting the hypothesis that the protoliths for the felsic rocks and eclogites in the Montagne Noire were tectonically associated prior to Variscan orogenesis.

In addition, zircon trace-element signatures (U/Yb– Hf and U/Yb–Y) in both dome-core and dome-margin eclogites indicate a continental affinity; eclogite protoliths were mafic (likely gabbroic) intrusions in continental crust (Whitney et al., 2020). Continental breakup and rifting of Gondwana in the Cambro-Ordovician (e.g. Pouclet et al., 2017) may have led to crustal thinning resulting in bimodal magmatism, with mafic underplating and partial melting of the overlying crust producing basaltic melts, cumulates, and depleted granulite at the base of the crust (Fig 8a). The CL-dark cores of zircons present little zoning (dome-core) to faint oscillatory zoning (dome-margin), and the relict euhedral shape of zircon cores in the dome-core eclogite are characteristic of igneous zircons. Th/U ~1.9 from dome-core eclogite zircon cores are likely indicative of magmatic mafic zircon (Teipel et al., 2004 & references therein). Dome-margin zircon Th/U < 0.8 would indicate formation from felsic to intermediate melts (e.g. Linnemann et al., 2011), which may reflect magmatic differentiation during mafic cumulate-forming processes. Combined with steep HREE slopes for all zircon cores, these Th/U values overall support an igneous protolith. Differences in Eu-anomalies between dome-core and dome-margin eclogite suggest that the mafic protoliths were petrogenetically distinct and formed by different

processes, such as forming from magma that differentially fractionated plagioclase or that were variably oxidized. The lack of Eu-anomaly in the dome-margin eclogite zircon cores points to a protolith derived from a melt that did not significantly fractionate plagioclase (Grimes et al., 2009; Hoskin and Schaltegger, 2003), or may indicate that the protolith was significantly oxidized (Trail et al., 2012) compared to the dome-core eclogite protoliths. In contrast, the pronounced negative Eu-anomaly in dome-core eclogite zircon cores suggests derivation from a more evolved plagioclase-bearing protolith.

Geochemical and textural differences between dome-core and dome-margin eclogites indicate different origins; differences are seen in zircon Th/U, rutile trace-element composition, and oxygen-isotope composition of zircon and garnet. Dome-core eclogite zircon cores show a wider spread of Th/U (<1.9), compared to more restricted zircon Th/U (<0.9) in the dome-margin. Rutile from the dome-core and dome-margin eclogites has distinct trace-element compositions, likely reflecting variation in protolith composition or history (e.g., cumulate processes).

Finally, $\delta^{18}O$ values measured in the CL-dark zircon cores of all eclogites, like zircon-core trace element compositions (Fig. 4c, d), are consistent with the protolith originating in a continental setting, with $\delta^{18}O$ values between ~8-9 ‰ in agreement with bulk values obtained from mafic lower crustal granulite xenoliths (Kempton and Harmon, 1992) and consistent with bulk O-isotope values from other late Variscan lithologies in the FMC (Downes et al., 1990, 1991). O-isotope fractionation between terrestrial silicate melts and crystallizing phases is small at magmatic temperatures (~1-2‰) (Eiler, 2001), so we assume that $\delta^{18}O$ values from zircon cores provide a reasonable basis for the protolith to be distinguished between a crustally-contaminated source and mantle-derived mafic melt origin. Zircon core $\delta^{18}O$ values are

maximum values, as slight mixing or O-diffusion from adjacent high-δ^{18}O domains in the rest of the grains or rock is also possible. Diffusion is slow in zircon at metamorphic temperatures <800ºC (Valley et al., 2003) but potentially relevant for zircon cores owing to the ~150 Myr separating protolith formation and H*P* metamorphism.

We therefore interpret the zircon core δ^{18}O values (TdF: 9.7‰, LJ: ~8.8‰, Cab: ~8.3‰) as maximum original δ^{18}O values acquired during zircon core crystallization in the protolith gabbro. Finally, zircons from these eclogites did not crystallize from an unaltered, mantle-derived MORB magma (~5.3‰, Valley et al., 1994), as would be expected from an oceanic MORB-basalt-derived protolith argued for by Pitra et al. (2021). In addition, seawater alteration of MORB-basalt at the ocean floor would lead to depressed δ^{18}O values rather than elevated ones (δ^{18}O SMOW ~ -4‰ at ~500 Ma, Kasting et al., 2006).

These observations support the hypothesis that the dome-margin and dome-core eclogite protoliths were emplaced in the same pre-orogenic crustal package but crystallized in different sections or at different stages in the crustal column prior to their shared eclogite-facies history. The eclogites and their protoliths formed in a continental (orogenic) setting and not during subduction.

6.2 Prograde metamorphism

Evidence for prograde metamorphism is present only in garnet zoning and inclusion distribution of dome-core eclogite (TdF, LJ). Cores of garnets are characterized by higher abundance of Fe, Mn and Ca relative to the Mg-rich rims. Garnet rims of dome-core eclogites formed during eclogite-facies metamorphism (Whitney et al., 2015), and garnet cores record a preceding episode of prograde metamorphism, likely in the amphibolite-facies. The lack of major-cation

zoning and presence of omphacite and rutile inclusions throughout garnets in the dome-margin eclogite indicate that dome-margin eclogites likely first nucleated and grew garnet at conditions not far from the eclogite-facies, consistent with deep emplacement of the protolith gabbro.

In contrast to dome-core eclogite garnets, zircon preserves a very sparse record of prograde metamorphic history. A few zircon cores from the TdF eclogite yielded U-Th-Pb dates of *c.* 360 Ma (Whitney et al., 2015), and Faure et al. (2014) obtained an Sm-Nd isochron date of 357.5 ± 8.6 Ma based in part on resorbed garnets. Owing to the extensive symplectization and therefore breakdown of high-Mg, eclogite-facies garnet rims in the retrogressed dome-core eclogite sample dated by Faure et al. (2014) (similar to the LJ eclogite, this study), we interpret the *c.* 360 Ma Sm-Nd date as that of prograde metamorphism recorded in the low-Mg, pre-eclogite facies garnet cores that were preserved and dated. An age of c. 360 Ma for prograde metamorphism for the eclogites coincides with the c. 360 Ma zircon core date obtained and interpreted as such by Whitney et al. (2015). In this context, the oldest *c.* 360 Ma zircon date of Pitra et al. (2021), interpreted by the authors as the age of eclogite-facies metamorphism, is more consistent with the timing of prograde metamorphism.

Although garnet in the dome-core eclogite is zoned in major and trace-element cations, little O-isotope zoning is present, and small variations do not systematically correlate with other element zoning. This lack of $\delta^{18}O$ zoning indicates no severe changes in fluid environment in the precursor phases consumed during garnet growth. Higher $\delta^{18}O$ values in the TdF eclogite relative to the LJ eclogite likely suggests either differences in the bulk $\delta^{18}O$ of the mafic protoliths or in isotopic exchange with the surrounding felsic lithologies.

6.3 Eclogite-facies metamorphism

6.3.1 Timing of eclogite-facies metamorphism

Evidence for eclogite-facies metamorphism is preserved in zircon rims and Type-II zircons, which we interpret either as neocrysts or as Type-Ia grains sectioned near the edge of the grain, and in garnet from both eclogite localities in the Montagne Noire (rim only in dome-core; entire garnets in dome-margin). Zircon U-Pb petrochronology results for all four samples show CL-bright rims crystallized *c.* 315-310 Ma, in agreement with Whitney et al. (2015, 2020). This Variscan age is systematically associated with flat HREE patterns and no Eu-anomaly features that are commonly interpreted as evidence for crystallization of metamorphic zircon (Th/U > 0.1) in garnet-present, plagioclase-absent conditions (e.g., Rubatto, 2002) defining the eclogite facies. In addition, Type-I zircons occur as inclusions in garnet in each eclogite (Supplement B), with rims yielding dates agreeing with the Variscan age we interpret as recording eclogite facies; this textural association would not be observed if these zircons recorded a late-fluid retrograde or L*P*-H*T* event accompanied by Pb-loss as suggested by Faure et al (2014) and Pitra et al. (2021), respectively.

In addition, the rutile U-Pb dates of 304.2 ± 5.7 Ma to 307.3 ± 4.5 Ma (and the less precise date of 320 ± 14 Ma obtained for the fresh dome-margin eclogite, CabF), are all consistent with the rutile age of 308 ± 4 Ma obtained by Faure et al. (2014) and are coeval with or slightly postdate the age of peak-*P* eclogite-facies metamorphism recorded by zircon, possibly indicating that rutile records cooling immediately following H*P* metamorphism. The observation that rutile in all samples records the same age is significant, and alongside the H*P* zircon data, confirms that all eclogites in the dome experienced broadly coeval H*P* metamorphism and exhumation.

6.3.2 Zircon behavior

More extensive zircon recrystallization and growth in the dome-core eclogites suggests that the eclogites experienced protracted high-temperature metamorphism and/or more prolonged interactions and more significant exchange with fluids sourced from the surrounding gneisses and migmatites; e,g., as a result of devolatilization and partial-melting reactions. Some TdF and LJ zircon cores are euhedral and surrounded by rims that nucleated at the original zircon boundary (Supplement A), suggesting mobilization of Zr and crystallization of new zircon templating on existing euhedral grains. These are distinct from the lobate growths of dome-margin zircon rims, possibly indicating limited dissolution-reprecipitation, a process facilitated by the fluids and/or melts (e.g. Geisler er al., 2007; Putnis, 2002; Ruiz-Agudo et al., 2014; Tomaschek et al., 2003). The more extensive recrystallization of dome-core eclogite zircon may have been facilitated by interaction with fluids and partial melt from the surrounding gneiss, resulting in more extensive zircon dissolution-reprecipitation and possibly new growth, in contrast to the very minimal zircon recrystallization at eclogite-facies in the dome-margin eclogite. The Montagne Noire eclogites have homogeneous Zr-contents of ~100-200 ppm (Whitney et al., 2020), typical of Phanerozoic continental basalts (Keller and Schoene, 2017), and therefore differences in extent of zircon recrystallization cannot be attributed to initial bulk-rock Zr content. These differences therefore most likely spring from variable interactions with fluids or melt derived from other lithologies at eclogite facies.

6.3.3 Zircon and garnet O-isotope signatures

The $\delta^{18}O$ signatures of zircon and garnet also distinguish the dome-core and dome-margin eclogites. Oxygen isotope fractionation between zircon and garnet is small (Valley et al., 2003), so we can compare their $\delta^{18}O$ values to assess equilibrium at the time of crystallization. We can utilize the garnet-zircon pair as a geochemical marker of fluid environment, assuming their $\delta^{18}O$ signature reflects the environment in which they crystallized, because intragranular diffusion of oxygen in garnet and zircon is extremely slow at metamorphic temperatures and relevant timescales (Valley et al., 1994; Vielzeuf et al., 2005; Watson & Cherniak, 1997). Although bulk rock $\delta^{18}O$ is not known, both zircon and garnet have domains that formed at eclogite-facies, and we consider their $\delta^{18}O$ values to reflect fluid signatures at these conditions.

Dome-margin eclogite zircon core, rim, and garnet $\delta^{18}O$ values overlap within error, suggesting growth from an unchanging fluid source in a relatively closed system, with little change in microchemical environment. In contrast, dome-core eclogites have zircon rim/Type-II $\delta^{18}O$ weighted mean values (TdF: 10.0 ± 0.1 / 10.2 ± 0.3‰; LJ: 9.2 ± 0.3 / 9.3 ± 0.2) higher than garnet $\delta^{18}O$ from these respective samples (TdF: 9.5 ± 0.3‰; LJ: 8.6 ± 0.1‰) (Table 2). In the LJ sample, zircon rim/Type-II $\delta^{18}O$ are higher than the zircon core average $\delta^{18}O$ value of 8.8 ± 0.1‰, and zircon cores and garnet in isotopic equilibrium ($1000\ln\alpha_{grt\text{-}zrn}$ ~0.1-0.2‰ at 700ºC for the measured range of garnet compositions, Valley et al., 2003). This suggests that dome-core eclogites more extensively interacted with fluids or partial melts from surrounding gneisses during zircon (re)crystallization, as compared to dome-margin eclogites.

To explain the young Montagne Noire H*P* zircon ages, distinct from older records of H*P* metamorphism in the FMC (~400 Ma, Faure et al., 2009; Lévézou: ~360 Ma, Najac: 380 Ma Lotout et al., 2018, 2020), Faure et al. (2014) invoked zircon growth from low-*P* shallow fluid alteration at 315-310 Ma, and Pitra et al. (2021) proposed that the age of H*P* metamorphism for

the Montagne Noire dome core eclogites was *c.* 360 Ma, corresponding to the upper limit of zircon U-Pb scatter between ~360-300 Ma, rather than the dominant group of analyses at ~310 Ma with flat HREE patterns. Pitra et al. (2021) argued that these younger dates must represent zircon U-Pb systematic resetting at inferred L*P* conditions, with a decoupling of U-Pb and REE systematics resulting in "deceptive" flat HREE patterns, not reflective of zircon recrystallization at eclogite facies.

Additionally, Pitra et al. (2021) did not account for the absence of an Eu-anomaly in Variscan zircon (equivalent to our Type-I zircon rims and Type-II zircons), which would be expected if these zircon domains had grown at low-*P* conditions, especially in retrogressed eclogite in which zircons are observed in symplectite domains that contain abundant plagioclase. Furthermore, zircon growth from low-*P*, shallow fluid alteration would produce depressed $\delta^{18}O$ values. Instead, the elevated $\delta^{18}O$ signature of zircon rims, in equilibrium with eclogite-facies garnet, supports our interpretation that zircon recrystallized at H*P* (eclogite-facies, plagioclase-absent) conditions and resulted from interactions with surrounding partially molten crust at *T* ~700°C prior to exhumation. We therefore maintain that the 315-310 Ma age most likely represents that of eclogite-facies metamorphism, coeval with the onset of migmatite crystallization.

6.4 Tracking eclogite source and trajectory

Previous paired garnet-zircon O-isotope studies in other metamorphic complexes have investigated protolith-to-metamorphic fluid-rock interactions in various tectonic settings, such as subduction zone metamorphism (e.g., Page et al., 2014, 2019), Alpine subduction of continental margin material (e.g. Sesia zone eclogites and metasediments, Vho et al., 2020), orogenic

settings (e.g. eclogites from the Western Gneiss Region, Russel et al., 2013), mantle-derived melt intrusions in migmatites (e.g. Pyrenes, Vielzeuf et al., 2005), and formation of eclogites at mantle depths (e.g. kimberlitic eclogites, Russell et al., 2013). Our measured $\delta^{18}O$ values between ~8-10.5‰ are consistent with bulk mafic granulite xenolith values from the base of the FMC crust (Downes et al., 1990), values up to 11‰ associated with quartzofeldspathic rocks and post-magmatic granites (Couzinié et al., 2016; Kempton & Harmon, 1992), and provide context for the likely $\delta^{18}O$ signature of other abundant lithologies in the FMC.

Although the Montagne Noire eclogites originated from the same continental magmatic province that produced gabbro intrusions, differences in their O-isotope values testify to their diverging metamorphic histories and trajectories (Figs. 8b, c). Uniform $\delta^{18}O$ values from dome-margin eclogites (Fig. 9) suggest little changes in fluid environment between protolith zircon formation and eclogite-facies recrystallization, consistent with a dry, eclogitized cumulate or restite that has not undergone much internal deformation or transport at depth. The lower temperatures obtained for the eclogite may indicate that H_2O was primarily locked in hydrous phases, observed as small amounts of epidote included in omphacite and garnet (Whitney et al., 2020), suggesting that available H_2O may not have been present as a free-fluid phase; i.e., consistent with less abundant and pervasive fluids. In the absence of fluids, the dome-margin rocks experienced a shorter period of reactivity or less favorable conditions for eclogitization at high-*P* conditions (e.g. Austrheim, 1987) with slightly lower-*T* at peak-*P* compared to the dome-core (Whitney et al., 2020), resulting in limited zircon recrystallization and homogeneous zircon $\delta^{18}O$ values. Dome-core eclogites underwent protracted and dynamic interactions with felsic lithologies at high-*T* conditions during crustal flow, with increased fluid and isotopic exchange

peaking at high-*P* and relatively high-*T*, leading to more extensive zircon recrystallization in the dome-core eclogite and acquisition of higher $\delta^{18}O$ values from prolonged interaction (Fig 9).

6.5 Geodynamic implications at the orogenic scale

Collision between Laurussia and Gondwana resulted in crustal thickening of a pre-orogenic crustal package (Fig. 8a) in the Variscan. Southward younging of late Variscan granitoid intrusions (Laurent et al., 2017) in the FMC suggests thickening of the orogenic plateau and southward flow of partially molten crust from the hinterland to the foreland (e.g. Faure et al., 2009; Vanderhaeghe et al., 2020), resulting in progressive deepening of the Moho in the southern margin of the orogen (Fig. 8b).

Consistent variations between radiogenic and stable isotope systems, major, trace elements, and REEs provide a robust framework to examine interactions in the deep Variscan crustal flow system (Fig. 8b, c). We propose that eclogitization of the dome-margin protolith resulted from *in situ* crustal thickening of the foreland driven by lateral *P*-gradients and resulting flow of deep crust at the dome emplacement location. The dome-core eclogite protolith underwent progressive burial (prograde metamorphism) starting in the center of the orogen, flowed towards the foreland and eclogitized in the thickened foreland between reaching its maximum burial depth and the onset of exhumation, as recrystallization at eclogite facies was aided by fluid-interactions with surrounding migmatites and deformation during flow (e.g. Austrheim, 1987) (Fig. 8b, c).

This proposed schematic reconstruction of orogenic eclogite origin and trajectory is in contrast to the geodynamic scenario proposed by Pitra et al. (2021), who interpreted the eclogites from the Montagne Noire as originating from oceanic crust that was subducted. The

Figure 8. Full-width page, Color

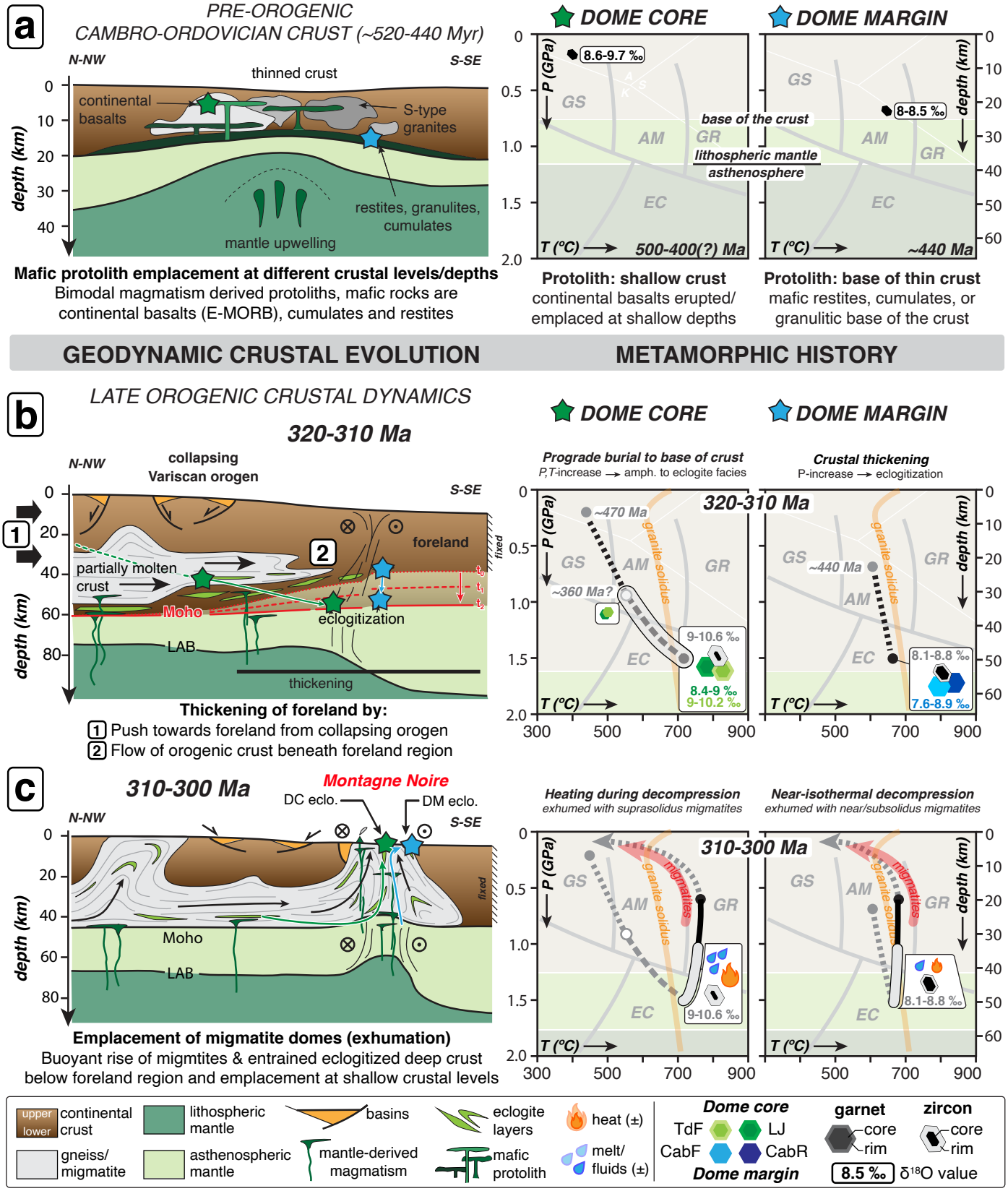

Figure 8. Proposed schematic geodynamic and metamorphic evolution of the Montagne Noire eclogites, from protolith to exhumation, showing their structural relationship and evolution withing the crustal architecture and associated metamorphic conditions (P, T, fluids). a) Schematic pre-orogenic Cambro-Ordovician setting with emplacement of mafic protolith in a thinned crust, and depth-position of protoliths within the crust; b) late orogenic crustal evolution of eclogite associated with thickening of the foreland region and deepening of the Moho, and deep crustal flow associated with distinct trajectories and magnitude of transport of dome-core and dome-margin eclogites as they reached eclogite-facies conditions from 320-310 Ma; c) exhumation of eclogites in the Montagne Noire dome and associated metamorphic conditions between 310-300 Ma. The 'flame' symbol indicates heat source at high-P from partially-molten migmatites and the 'water drop' symbol indicates source of fluids for zircon recrystallizing at high-P from partially molten migmatites and/or fluids driven off as a result of their partial melting.

interpretation of oceanic basaltic origin for the eclogites and H*P* metamorphism resulting from subduction led Pitra et al. (2021) to generate a geodynamic dilemma in the broader context of the Variscan FMC architecture: subduction during the late stages of the Variscan orogeny at *c.* 315-310 Ma is unlikely. This led the authors to interpret the oldest date of *c.* 360 Ma obtained from their zircon analyses as that of H*P* metamorphism, reconciling the presence of eclogites in the Montagne Noire by invoking southward lateral migration of the eclogites at *c.* 315-310 Ma during the L*P* events associated with migmatization, despite the associated flat HREE signatures of eclogite zircons that must, in their view, be decoupled from the U-Pb systematics to explain the presence of eclogite-facies zircons with a Variscan age.

We have examined the evidence of when and where eclogites formed in the FMC without a preconceived idea for the tectonic setting of the eclogite protolith and the relative timing of eclogitization and migmatization. We provide an alternative and more likely geodynamic scenario for the history of the eclogites based on textural observations, petrochronology and oxygen-isotope results. This approach indicates that (1) the eclogite protolith is of continental origin based on geochemical data, including the O-isotope signatures of zircon and garnet, as well as by the similar protolith ages and timing of metamorphism recorded by the eclogites and the host gneiss and migmatite, and (2) textural and geochemical variations between dome-core and dome-margin eclogites suggest that their deep crustal history and interactions with partially molten gneiss and migmatite in the deep crust differed in terms of the extent of interaction with partial-melt derived fluids prior to exhumation. Finally, following lateral flow in the deep crust – significant in the case of the dome-core eclogite and less so for the dome-margin eclogite – both eclogites were dragged toward the median (dome-core) high-strain zone that acted as an efficient exhumation pathway during extension/transtension that drove exhumation of the deep crust in a

Figure 9. Full-width page, Color

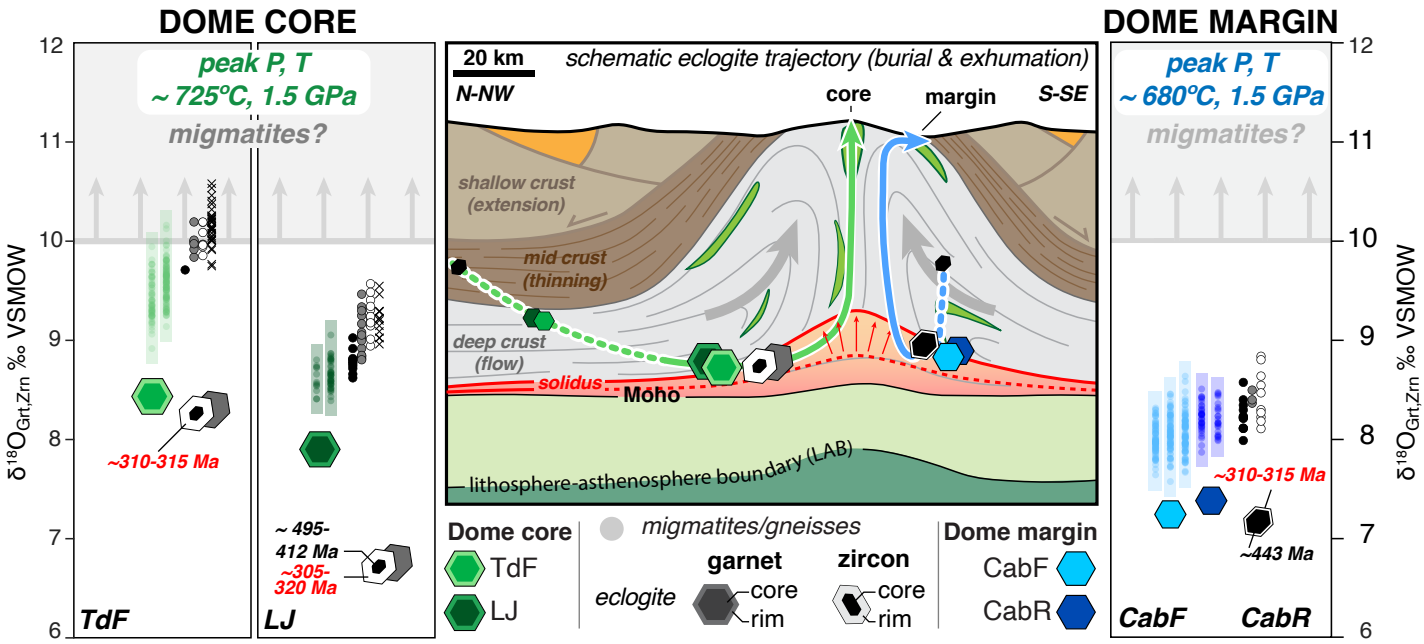

Figure 9. Schematic cross section of proposed eclogite trajectories from protolith to eclogite-facies and subsequent exhumation. Dome-core O-isotope and U-Pb petrochronology data is summarized on the left, and dome-margin data is summarized on the right, showing the $\delta^{18}O$ values measured in the eclogites compared to the likely $\delta^{18}O$ signature of migmatites proposed to have variably interacted with eclogites emplaced at different locations in the dome.

migmatite dome (Rey et al., 2009a, b, 2011, 2017; Whitney et al., 2013, 2020; Korchinski et al., 2018); the dome-margin eclogite experienced additional transport away from this zone in the shallow crust, whereas the dome-core eclogite remained within the high-strain zone (Fig. 9).

Conclusions

Eclogites from the Montagne Noire dome are continental eclogites with Cambro-Ordovician protoliths (~520-400 Ma) derived from variously evolved mafic melts that crystallized as distinct gabbroic intrusions, and subsequently eclogitized in the deep crust during the Variscan orogeny. Both mafic protoliths underwent eclogitization at ~315-310 Ma (U-Pb: zircon rims, rutile) and variably interacted with the surrounding gneiss/migmatite, as recorded by paired oxygen-isotope analysis of eclogite-facies minerals, resulting in different extents of zircon (re)crystallization.

The record of coeval eclogitization of deep mafic crust and migmatite crystallization in the Montagne Noire dome indicates that both were deeply sourced, even if only the eclogites record the H*P* conditions. This suggests that much of the material composing the Montagne Noire and perhaps other gneiss domes may be derived from much greater depths than the felsic bulk of orogens records. This study of eclogites from the Montagne Noire provides an exceptional window into deep crustal dynamics and processes, recording fluid exchange and interactions between mafic and felsic rocks at eclogite facies.

Acknowledgements

Funding for this project comes from NSF grants EAR-1050020 and EAR-1946911 to Whitney and Teyssier, as well as funding from the College of Science and Engineering at the University of Minnesota. Funding for the electron microprobe facility used in this research was provided by

NSF grant EAR-1625422. SIMS analyses were carried out at the University of Madison-Wisconsin department of Geology, WiscSIMS is supported by NSF (EAR2004618) and the University of Wisconsin-Madison. We thank Patrice Rey for collaborative field work to locate and collect the dome-core eclogites, Andrew Kylander-Clark for assistance with LASS-ICP-MS analyses and data processing at the University of Santa Barbara, and Natalie H. Raia as SHRIMP-II zircon data analyst. We also thank John V. Valley and Michael Spicuzza at the University of Madison-Wisconsin, as well as Michelle Gevedon for advice and assistance with sample preparation and Kouki Kitajima for remote analytical session planning, instrument tuning, and SIMS O-isotope data collection. We would also like to thank Mr. Daniel Daures of Le Teil Farm for his help with the search and collection of eclogite samples from the Cabardès area; Mr. Robert Pistre and the Centre de Recherche du Patrimoine de Rieumontagné (CRPR), as well as the association Les Amis des Sciences de la Nature (ASNAT), for their work archiving the work carried out by M. Demange during his career, including unpublished maps and documents, all of which were an invaluable resource in our work in the Montagne Noire.

REFERENCES:

1. Aerden, D.G.A.M., 1998. Tectonic evolution of the Montagne Noire and a possible orogenic model for syncollisional exhumation of deep rocks, Variscan belt, France. Tectonics 17, 62-79.
2. Arab, A., Godard, G., Ouzegane, K. Acosta-Vigil, A., Kiénast, J.-R., Román-Alpiste, MJ., Garrido, C.J., Drareni, A. 2021. Partial melting and P-T evolution of eclogite-facies metapelitic migmatites from the Egere terrane (Central Hoggar, South Algeria). American Mineralogist 106, 1209-1224.
3. Austrheim, H., 1987. Eclogitization of lower crustal granulites by fluid migration through shear zones. Earth and Planetary Science Letters 81, 221-232.
4. Baldwin, S.L., Monteleone, B.D., Webb, L.E., Fitzgerald, P.G., Grove, M., Hill, E.J., 2004. Pliocene eclogite exhumation at plate tectonic rates in eastern Papua New Guinea. Nature 431, 263-267. https://doi.org/10.1038/nature02846
5. Bodinier, J.L., Burg, J.P., Leyreloup, A., Vidal, H., 1988. Reliques d'un basin d'arrière-arc subducte, puis obducte dans la region de Marvejols (Massif Central). Bulletin de la Société Géologique de France 1, 21-33.
6. Bouchardon, J.L., Déchomets, R., Demange, M., 1979. A propos du disthène en roche dans les micaschistes et les gneiss du synclinal de Rosis et du flanc sud, zone axiale de la Montagne Noire (Massif Central français). Comptes rendus de l'Académie des Sciences, D 288, 1067-1071.
7. Brueckner, H. K., 2018. The great eclogite debate of the Western Gneiss Region, Norwegian Caledonides: The in situ crustal v. exotic mantle origin controversy. Journal of Metamorphic Geology 46(5), 517-527.

8. Cabanis, B., Godard, G., 1987. Les éclogites du pays de Léon (Nord-Ouest du Massif Armoricain): étude pétrologique et géochimique; implications géodynamiques. Bulletin de la Société Géologique de France 8, 1133-1142.
9. Couzinié, S., Laurent, O., Moyen, J.F., Zeh, A., Bouilhol, P., Villaros, A., 2016. Post-collisional magmatism: crustal growth not identified by zircon Hf–O isotopes. Earth and Planetary Science Letters 456, 182-195
10. Cuthbert, S.J., Carswell, D.A., Krogh-Ravna, E.J., Wain, A., 2000. Eclogite and eclogites in the Western Gneiss Region, Norwegian Caledonides. Lithos 52, 165-195.
11. Demange, M., 1985. The eclogite-facies rocks of the Montagne Noire, France. Chemical Geology 50, 173-188.
12. Demange, M., 1994. Antevariscan evolution of the Montagne noire (France): from a passive margin to a foreland basin, Comptes rendus de l'Académie des Sciences 318, 921-933.
13. Demange, M., Guérangé-Lozes, J., Guérangé, B., 1996. Carte géologique de Lacaune et sa notice. Carte géologique de la France au 1:50000 n8987. Bureau de Recherches Géologiques et Minières, Orléans, France.
14. Doublier, M.P., Potel, S., Wemmer, K., 2014. The tectono-metamorphic evolution of the very low-grade hangingwall constrains two-stage gneiss dome formation in the Montagne Noire (Southern France). Journal of Metamorphic Geology 33, 71-89.
15. Downes, H., Dupuy, C., Leyreloup, A.F., 1990. Crustal evolution of the Hercynian belt of Western Europe: Evidence from lower crustal granulite xenoliths (French Massif Central). Chemical Geology 83, 209-231

16. Downes, H., Kempton, P.D., Briot, D., Harmon, R.S., 1991. Pb- and O-isotope systematics in granulite facies xenoliths, French Massif Central: Implications for crustal processes. Earth and Planetary Science Letters 102, 342-357.
17. Eiler, J.M., 2001. Oxygen isotope variations of basaltic lavas and upper mantle rocks. Reviews in Mineralogy and Geochemistry 43, 319-364.
18. Eskola, P.,1921. On the eclogites of Norway. Videnskapsselskapets Skrifter. I-Mathematisk-Naturvidenskapelig Klasse (Kristiana), 1-118.
19. Faure, M., Lardeaux, J.-M., Ledru, P., 2009. A review of the pre-Permian geology of the Variscan French Massif Central. Comptes Rendus Geoscience 341, 202-213.
20. Faure, M., Cocherie, A., Gaché, J., Esnault, C., Guerrot, C., Rossi, P., Wei, L., Qiuli, L., 2014. Middle Carboniferous intracontinental subduction in the Outer Zone of the Variscan Belt (Montagne Noire Axial Zone, French Massif Central): multimethod geochronological approach of polyphase metamorphism, in: Schulmann, K., Martinez Catalan, J.R., Lardeaux, J.M., Janousek, V., Oggiano, G. (Eds.), The Variscan orogeny: Extent, timescale and the formation of the European crust. Geological Society of London Special Publications 405, 289-311.
21. Ferrero, A., Ague, J. J., O'Brien, P. J., Wunder, B., Remusat, L., Ziemann, M. A., Axler, J., 2021. High-pressure, halogen-bearing melt preserved in ultrahigh-temperature felsic granulites of the Central Maine Terrane, Connecticut (U.S.A.) American Mineralogist 106, 1225-1236.
22. Franke, W., Doublier, M.P., Klama, K., Potel, S., Wemmer, K., 2011. Hot metamorphic core complex in a cold foreland. International Journal of Earth Sciences 100, 753-785.

23. Fréville, K., Cenki-Tok, B., Trap, P., Rabin, M., Leyreloup, A., Régnier, J.-L., Whitney, D. L., 2016. Thermal interaction of middle and upper crust during gneiss dome formation: Example from the Montagne Noire (French Massif Central). Journal of Metamorphic Geology 34, 447-462.
24. Geisler, T., Schaltegger, U., Tomaschek, F., 2007. Re-equilibration of zircon in aqueous fluids and melts. Elements 3, 43-50.
25. Géze, B., 1949. Etude géologique de la Montagne Noire et les Cévennes méridionales. Mémoires de la Société géologique de France 29 (62). 215 pp.
26. Grimes, C.B., John, B.E., Kelemen, P.B., Mazdab, F.K., Wooden, J.L., Cheadle, M.J., Hanghoj, K., Schwartz, J.J., 2007. Trace element chemistry of zircons from oceanic crust: a method for distinguishing detrital zircon provenance. Geology 35, 643-646.
27. Grimes, C.B., John, B.E., Cheadle, M.J, Mazdab, FK, Wooden, J.L., Swapp, S., Schwartz, J., 2009. On the occurrence, trace element geochemistry, and crystallization history of zircon from in situ ocean lithosphere. Contributions to Mineralogy and Petrology 158, 757-783.
28. Groppo, C., Rolfo, F., Liu, Y.-C., Deng, L.-P., Wang, A.-D., 2015. P-T evolution of elusive UHP eclogites from the Luotian dome (North Dabie Zone, China): How far can the thermodynamic modeling lead us? Lithos 226, 183-200. https://doi.org/10.1016/j.lithos.2014.11.013
29. Herwartz, D., Nagel, T. J., Münker, C., Scherer, E. E., Froitzheim, N., 2011. Tracing two orogenic cycles in one eclogite sample by Lu–Hf garnet chronometry. Nature Geoscience 4, 178-183.

30. Hoskin, P.W.O., Schaltegger, U., 2003. The composition of zircon and igneous and metamorphic petrogenesis. Reviews in Mineralogy and Geochemistry 53(1), 27-62.
31. Kasting, J.F., Howard, M. T., Wallmann, K., Veizer, J., Shields, G., Jaffrés, J., 2006. Paleoclimates, ocean depth, and the oxygen isotopic composition of seawater. Earth and Planetary Science Letters 252, 82-93.
32. Keller, B., Schoene, B., 2017. Plate tectonics and continental basalt geochemistry through Earth history. Earth and Planetary Science Letters 481, 290-304.
33. Kempton, P.D., Harmon, R.S., 1992. Oxygen isotope evidence for large-scale hybridization of the lower crust during magmatic underplating. Geochimica Cosmochimica Acta 56, 971-986.
34. Kita, N.T., Ushikubo, T., Fu, B.,Valley J. W., 2009. High precision SIMS oxygen isotope analyses and the effect of sample topography. Chemical Geology 264, 43-57.
35. Korchinski, M., Rey, P.F., Mondy, L., Teyssier, C., Whitney, D.L., 2018. Numerical investigation of deep-crust behavior under lithospheric extension. Tectonophysics 726, 137-146.
36. Kylander-Clark, A.R.C., Hacker, B.R.,Cottle, J.M., 2013. Laser-ablation split-stream ICP petrochronology. Chemical Geology 345, 99-112.
37. Laurent, O., Couzinié, S., Zeh, A., Vanderhaeghe, O., Moyen, J. F., Villaros, A., Gardien, V., Chelle-Michou, C., 2017. Protracted, coeval crust and mantle melting during Variscan late-orogenic evolution: U–Pb dating in the eastern French Massif Central. International Journal of Earth Sciences 106, 421-451.
38. Linnemann, U., Ouzegane, K., Drareni, A., Hoffmann, M., Becker, S., Gärtner, A., Sagawe, A., 2011. Sands of West Gondwana: An archive of secular magmatism and plate

interactions — A case study from the Cambro-Ordovician section of the Tassili Ouan Ahaggar (Algerian Sahara) using U–Pb–LA-ICP-MS detrital zircon ages. Lithos 123, 188-203.

39. Little, T. A., Hacker, B. R., Gordon, S. M., Baldwin, S. L., Fitzgerald, P. G., Ellis, S., Korchinski, M., 2011. Diapiric exhumation of Earth's youngest (UHP) eclogites in the gneiss domes of the D'Entrecasteaux Islands, Papua New Guinea. Tectonophysics 510, 39-68.
40. Lotout, C., Pitra, P., Poujol, M., Anczkiewicz, R., Van Den Driessche, J., 2018. Timing and duration of Variscan high-pressure metamorphismin the French Massif Central: A multimethod geochronological study from the Najac Massif. Lithos 308, 381-394.
41. Lotout, C., Poujol, M., Pitra, P., Anczkiewicz, R., van den Driessche, J., 2020. From burial to exhumation: emplacement and metamorphism of mafic eclogitic terranes constrained through multimethod petrochronology, case study from the Lévézou massif (French Massif Central, Variscan belt). Journal of Petrology 61, 1-27.
42. Möller, C., Andersson, J., Dyck, B., Lundin, I.A., 2015. Exhumation of an eclogite terrane as a hot migmatitic nappe, Sveconorwegian orogen. Lithos 226, 147-168.
43. O'Brien, P.J., 2019. Tso Morari coesite eclogite: pseudosection predictions v. the preserved record and implications for tectonometamorphic models. Geological Society of London Special Publications 474, 5-24.
44. Page, F.Z., Kita, N.T., Valley, J.W., 2010. Ion microprobe analysis of oxygen isotopes in garnets of complex chemistry. Chemical Geology 270, 9-19.

45. Page, F.Z., Essene, E.J., Mukasa, S.B., Valley, J.W., 2014. A garnet-zircon oxygen isotope record of subduction and exhumation fluids from the Franciscan Complex, California. Journal of Petrology 55, 103-131.
46. Page, F.Z., Cameron, E.M., Flood, C.M., Dobbins, J.W., Spicuzza, M.J., Kitajima, K., Strickland, A., Ushikubo, T., Mattison, C.G., Valley, J.V., 2019. et al., 2019; Extreme oxygen isotope zoning in garnet and zircon from a metachert block in mélange reveals metasomatism at the peak of subduction metamorphism. Geology 47, 655-658.
47. Paquette, J.-L., Ballèvre, M., Peucat, J.-J., Cornen, G., 2017. From opening to subduction of an oceanic domain constrained by LA-ICP-MS U-Pb zircon dating (Variscan belt, Southern Armorican Massif, France). Lithos 294, 418-437.
48. Pitra, P., Poujol, M., Van Den Driessche, J., Bretagne, E., Lotout, C., Cogné, N., 2021. Late Variscan (315 Ma) subduction or deceptive zircon REE patterns and U–Pb dates from migmatite-hosted eclogites? (Montagne Noire, France). Journal of Metamorphic Geology 00, 1–27. doi: 10.1111/jmg.12609
49. Pouclet, A., Álvaro, J.J., Bardintzeff, J.-M., Imaz, A.G., Monceret, E., Vizcaïno, D., 2017. Cambrian-early Ordovician volcanism across the South Armorican and Occitan domains of the Variscan Belt in Farnce: Continental break-up and rifting of the northern Gondwana margin. Geoscience Frontiers 8, 25-64.
50. Poujol, M., Pitra, P., Van Den Driessche, J., Tartèse, R., Ruffet, G., Paquette, J.-L., Poilvet, J.-C., 2017. Two-stage partial melting during the Variscan extensional tectonics (Montagne Noire, France). International Journal of Earth Sciences 106, 477-500.
51. Putnis, A., 2002. Mineral replacement reaction: from macroscopic observations to microscopic mechanisms. Mineralogical Magazine 66, 689-708.

52. Rabin, M., Trap, P., Carry, N., Fréville, K., Cenki-Tok, B., Lobjoie, C., Goncalves, P., Marquer, D., 2015. Strain partitioning along the anatectic front in the Variscan Montagne Noire massif (Southern French Massif Central). Tectonics 34, 1709-1735.
53. Rey, P.F., Teyssier, C., Whitney, D.L., 2009a. Extension rates, crustal melting, and core complex dynamics. Geology 37, 391-394.
54. Rey, P.F., Teyssier, C., Whitney, D.L., 2009b. The role of partial melting and extensional strain rates in the development of metamorphic core complexes. Tectonophysics 477, 135-144.
55. Rey, P.F., Teyssier, C., Kruckenberg, S.C., Whitney, D.L., 2011. Viscous collision in channel explains double domes in metamorphic core complexes. Geology 39, 387–390.
56. Rey, P.F., Mondy, L., Duclaux, G., Teyssier, C., Whitney, D.L., Bocher, M., Prigent, C., 2017. The origin of contractional structures in extensional gneiss domes. Geology 45, 263-266.
57. Roger, F., Respaut, J.-P., Brunel, M., Matte, P., Paquette, J.-L., 2004. Première datation U–Pb des orthogneiss oeillés de la zone axiale de la Montagne Noire (Sud du Massif Central): nouveaux témoins du magmatisme ordovicien dans la chaîne varisque, Comptes Rendus Géosciences 336, 19-28.
58. Roger, F., Teyssier, C., Respaut, J.-P., Rey, P.F., Jolivet, M., Whitney, D.L., Paquette, J.-L., Brunel, M., Matte, P., 2015. Emplacement of anatectic granite during Variscan extension and exhumation of the Montagne Noire double dome, French Massif Central, France. Tectonophysics 640–641, 53-69.
59. Roger, F., Teyssier, C., Whitney, D.L., Respaut, J.-P., Paquette, J.-L., Rey, P.-F., 2020. Age of metamorphism and deformation in the Montagne Noire dome (French Massif Central):

Tapping into the memory of fine-grained gneisses using monazite U-Th-Pb geochronology. Tectonophysics 776, 228-3136

60. Rubatto, D., 2002. Zircon trace element geochemistry: distribution coefficients and the link between U–Pb ages and metamorphism. Chemical Geology 184, 123-138.

61. Ruiz-Agudo, E., Putnis, C. V., Putnis, A., 2014. Coupled dissolution and precipitation at mineral–fluid interfaces. Chemical Geology 282, 132-146.

62. Russell, A.K., Kitajima, K., Strickland, A., Medaris, L.G., Schulze, D.J., Valley, J.W., 2013. Eclogite-facies fluid infiltration: constraints from $\delta^{18}O$ zoning in garnet. Contributions to Mineralogy and Petrology 165, 103-116.

63. Schuiling, R.D., 1960. Le dôme gneissique de l'Agout (Tarn et Hérault). Mémoires de la Société géologique de France 39, 1-59.

64. Shao, T., Xia, Y., Ding, X., Cai, Y., Song, M., 2019. Zircon saturation model in silicate melts: a review and update. Acta Geochimica 39, 238-403.

65. Štípská. P., Schulmann, K., Powell, R., 2008. Contrasting metamorphic histories of lenses of high-pressure rocks and host migmatites with a flat orogenic fabric (Bohemian Massif, Czech Republic): A result of tectonic mixing within horizontal crustal flow? Journal of Metamorphic Geology 26, 623-646.

66. Teipel, U., Eichhorn, R., Loth, G., Rohrmüller, J., Höll, R., Kennedy, A., 2004. U-Pb SHRIMP and Nd isotopic data from the western Bohemian Massif (Bayerischer Wald, Germany): Implications for Upper Vendian and Lower Ordovician magmatism. International Journal of Earth Sciences 93, 782-201.

67. Thompson, P.H., Bard, J.-P., 1982. Isograds and mineral assemblages in the eastern axial zone, Montagne Noire (France): Implications for temperature gradients and P-T history. Canadian Journal of Earth Sciences 19, 129-141.
68. Tomaschek, F., Kennedy, A. K., Villa, I. M., Lagos, M., Ballhaus, C., 2003. Zircons from Syros, Cyclades, Greece–Recrystallization and mobilization of zircon during high-pressure metamorphism. Journal of Petrology 44, 1977-2002.
69. Tomkins, H.S., Powell, R., Ellis, D.J., 2007. The pressure dependence of the zirconium-in-rutile thermometer. Journal of Metamorphic Geology 25, 703-713. https://doi.org/10.1111/j.1525-1314.2007.00724.x
70. Trail, D., Watson, E.B., Tailby, N.D., 2012. Ce and Eu anomalies in zircon as proxies for the oxidation state of magmas. Geochimica et Cosmochimica Acta 97, 70-78.
71. Trap, P., Roger, F., Cenki-Tok, B., Paquette, J.-L., 2017. Timing and duration of partial melting and magmatism in the Montagne Noire gneiss dome (French Massif Central). International Journal of Earth Sciences 106, 453-476.
72. Valley J.W., Chiarenzelli J.R., McLelland J.M., 1994. Oxygen isotope geochemistry of zircon. Earth and Planetary Science Letters 126, 187-206.
73. Valley, J.W., Bindeman, I.N., Peck, W.H., 2003. Empirical calibration of oxygen isotope fractionation in zircon. Geochimica et Cosmochimica Acta 67, 3257-3266.
74. Valley, J.W, Kita, N.T., 2009. In situ oxygen isotope geochemistry by ion microprobe. *In* Secondary Ion Mass Spectrometry in the Earth Sciences: Gleaning the Big Picture from a Small Spot 41 (Eds. M. Fayek). Mineralogical Association of Canada Short Course Series, 19–63.

75. Vanderhaeghe, O., Laurent, O., Gardien, V., Moyen, J.-F., Gébelin, A., Chelle-Michou, C., Couzinié, S., Villaros, A., Bellanger, M., 2020. Flow of partially molten crust controlling construction, growth and collapse of the Variscan orogenic belt: the geologic record of the French Massif Central. Bulletin de la Société Géologique de France 191, 1-56.
76. Vho, A., Rubatto, D., Lanari, P., Giuntoli, F., Regis, D., Herman, J., 2020. Crustal reworking and hydration: insights from element zoning and oxygen isotopes of garnet in high-pressure rocks (Sesia Zone, Western Alps). Contributions to Mineralogy and Petrology 175. https://doi.org/10.1007/s00410-020-01745-6
77. Vielzeuf, D., Veschambre, M., Brunet, F., 2005. Oxygen isotope heterogeneities and diffusion profile in composite metamorphic-magmatic garnets from the Pyrenees. American Mineralogist 90, 463-472
78. Watson, E.B., Cherniak, D.J., 1997. Oxygen diffusion in zircon. Earth and Planetary Science Letters 148, 527-544.
79. Whitney, D.L., Teyssier, C., Rey, P.F., Buck, W.R., 2013. Continental and oceanic core complexes. Geological Society of America Bulletin 125, 273-298.
80. Whitney, D.L., Roger, F., Teyssier, C., Rey, P.F., Respaut, J.-P., 2015. Syn-collapse eclogite metamorphism and exhumation of deep crust in a migmatite dome: The P-T-t record of the youngest Variscan eclogite (Montagne Noire, French Massif Central). Earth and Planetary Science Letters 430, 224-234.
81. Whitney, D.L., Hamelin, C., Teyssier, C., Raia, N.H., Korchinski, M.S., Seaton, N.C.A., Bagley, B.C., von der Handt, A., Roger, F., Rey, P.F., 2020. Deep crustal source of gneiss dome revealed by eclogite in migmatite (Montagne Noire, French Massif Central. Journal of Metamorphic Geology 38, 297-327.

82. Zheng, Y.-F., Zhao, Z.-F., Chen, R.-X., 2018. Ultrahigh-pressure metamorphic rocks in the Dabie-Sulu orogenic belt: compositional inheritance and metamorphic modification. Geological Society of America Special Publications 474, 89-132.

LIST OF TABLES:

LIST OF FIGURES:

LIST OF SUPPLEMENTARY INFORMATION FILES

Appendix A

Appendix B

- Table B: Zircon LASS-ICP-MS data
- Figure B1: post-ablation CL images of TdF zircons
- Figure B2: post-ablation CL images of LJ zircons
- Figure B3: post-ablation CL images of CabR zircons

Appendix C

- Table C: LJ eclogite zircon SHRIMP-II data
- Figure C: Zircon SHRIMP-II U-Pb petrochronology

Appendix D

- Table D: Rutile LASS-ICP-MS data

Appendix E:

- Table E1: Garnet $\delta^{18}O$ calibration curve determination for SIMS analyses
- Table E2: Garnet $\delta^{18}O$ SIMS data
- Table E3: Zircon $\delta^{18}O$ SIMS data

Appendix F:

- Table F1: EPMA Reference Materials/Standards used for MAN background correction used in quantitative garnet maps
- Tables F2-F10: Individual garnet EPMA map quantitative data

TABLES AND FIGURE CAPTIONS

Table 1. Summary of U-Pb petrochronology (LASS-ICP-MS) results. U-Pb petrochronology: averaged values are reported and marked in tables B (zircon) and table D (rutile).

Table 2. Summary of O-isotope data analysis (SIMS) results. Weighted mean $\delta^{18}O$ values for individual garnet grains and distinct zircon domains are given for all four eclogite samples analyzed, with the error reported at 95% confidence; for dispersed analytical groups, dispersion is reported and 95% conf. region of the dispersion (1.96×ω). Full dataset can be found in Table E.

Figure 1. Simplified geologic map of the Montagne Noire (upper left inset: relationship to Variscan exposures in yellow: IB = Iberian, PYR = Pyrenees, ARM = Armorican, and MC = Massif Central) after Whitney et al. (2020) and references therein, showing the distribution of eclogite localities and samples used in this study. Schematic foliation trends in the Axial Zone of the Montagne Noire are represented by curved grey lines; anatectic granitic intrusions are represented in dark grey on the map (S = Soulié, V = Vialais). Eclogite samples are identified as follows – dome-core samples: TdF = Terme de Fourcaric, LJ = Le Jounié (green stars); dome-margin samples: Cab = Cabardès (blue star). Representative thin section images of all four eclogite samples are shown in the left (dome-margin) and right (dome-core) panels, with fresh eclogites TdF and CabF (F = Fresh) at top, and retrogressed eclogites LJ and CabR (R = Retrogressed) on the bottom. Lower right inset highlights main structural subdomains of the

Axial zone in relationship to eclogite localities. GPS coordinated for all samples in this study: Whitney et al., (2020), Table 1.

Figure 2. Representative textures of eclogites. Dome-core: a) top: backscatter electron (BSE) image of the TdF eclogite; left: plane-polarized light (PPL) image of subhedral garnet with quartz-inclusion-rich cores and inclusion-poor rutile-bearing rims; right: PPL image of matrix omphacite with extremely fine-grained (grey) symplectites after omphacite, rutile present in the matrix; b) BSE image of LJ retrogressed eclogite, dotted lines represent the original garnet-matrix boundary, matrix is entirely symplectite after omphacite (Smp_1), garnet grains have undergone extensive partial replacement at the rim (Smp_2); left: cross-polarized light (XPL) image of Smp_1 and Smp_2 symplectite domains. Smp_{2a} and Smp_{2b} represent different garnet replacement symplectite assemblages; right: PPL image of matrix rutile partially replaced by titanite at the rim and surrounded by fine-grained Smp_1 phases. Dome-margin: c) BSE image of CabF eclogite highlighting bimodal garnet size distribution; left: PPL image of a large garnet grain with numerous inclusions of omphacite and few hornblende inclusions; right: PPL image of well-preserved matrix omphacite with limited symplectization at omphacite grain boundaries; rutile and hornblende present in the matrix; d) BSE image of CabR retrogressed eclogite; left: PPL image of a large garnet grain with abundant omphacite and rutile inclusions, similar to CabF but with extensive replacement of omphacite by symplectite in the matrix; right: PPL image of coarse-grained biotite and hornblende grains in the matrix, with relict omphacite partially replaced by fine-grained symplectite.

Figure 3. Zircon U-Pb petrochronology. Dome-core – TdF: (a)-(d), LJ: (e)-(h); Dome-margin – Cab: (i)-(l). a,e,i): CL-images of representative zircons, analytical spots with associated U-Pb dates and Th/U values for TdF, LJ, and Cab eclogites respectively, b,f,j) distribution of ^{207}Pb-corrected ^{238}U/^{206}Pb dates separated by textural association of analyzed zircons in TdF, LJ, and Cab eclogites respectively; c,g,k) Tera-Wasserburg plots of TdF zircon analyses and calculated concordia ages for zircon-rim and zircon-core analyses, where applicable, for TdF, LJ, and Cab eclogites respectively; MSDW given as MSWD of concordance + equivalence. Ellipses drawn are not corrected for common-Pb; however, for discordant or isolated analyses, ^{238}U/^{206}Pb date ranges are given after common-Pb correction on individual spots using the ^{207}Pb method (see Table B). Arrows indicate the location of zircon rim (green) and core (purple) analyses associated with corresponding date ranges or calculated concordia ages (boxed); d) chondrite-normalized REE plots of individual spot analyses color-coded by ^{207}Pb-corrected ^{238}U/^{206}Pb dates for in TdF, LJ, and Cab eclogites respectively (plotted patterns indicated in Table B).

Figure 4. Zircon trace-element compositions. a) Th/U vs. U-Pb dates for dome-core eclogite zircons, vertical line at Th/U = 0.1 represents value commonly used to distinguish metamorphic (low Th/U < 0.1) from igneous (high Th/U > 0.1) zircon fields, along with U-Pb ages and REE patterns (Rubatto, 2002); b) dome-margin eclogite zircons; c) Y (ppm) vs. U/Yb and, d) Hf (ppm) vs. U/Yb plots of all LASS-ICP-MS zircon analyses, with individual spot analyses color-coded by ^{207}Pb-corrected ^{238}U/^{206}Pb dates. Continental and oceanic crust zircon fields from Grimes et al. (2007).

Figure 5. Rutile U-Pb petrochronology and trace-element compositions. Rutile Tera-Wasserburg plots for a) TdF, b) LJ, c) CabF, and d) CabR eclogites, with lower-intercept ages and y-intercept values calculated indicated for each sample. Rutile trace-element compositions: e) Nb (ppm) vs. Cr (ppm) and f) Zr (ppm) vs. U (ppm) plots showing distinct grouping of rutile compositions for dome-core vs. dome-margin eclogites.

Figure 6. Zircon O-isotopes. Measured $\delta^{18}O$ values and associated 2SD error for individual spot analyses in a) TdF, b LJ and c) CabR eclogites. Top row: analyses plotted as 'per-grain basis' (white line between groups of analyses separates different grains analyzed); Middle row: compounded analyses plotted as 'per-domain basis' (T-I zircons: core, mantle, rim; T-II zircons: center, edge of grains); Bottom row: CL-images of representative Type-I and Type-II grains of TdF (a), LJ (b) and CabR (c) eclogites. U-Pb ages from this study and from the literature are indicated for zircon core (purple) and rim (green) domains. U-Pb ages: (*) this study, (≠)Whitney et al. (2015), (≠)Whitney et al. (2020).

Figure 7. Garnet O-isotope and major-element compositions. a) ternary garnet composition plots for each sample and analyzed garnet (color coded by sample: green = dome-core, blue = dome-margin), garnet compositions with measured $\delta^{18}O$ values in garnet composition space, and ternary plots showing the range of $\delta^{18}O$ values for individual samples; (b)-(e) Mg-Kα EPMA map (left), calculated quantitative pyrope map overlain on BSE image (center), and $\delta^{18}O$ traverses and associated garnet end-member compositions of texturally representative garnets (right) in the a) TdF, b) LJ, c) CabF, and d) CabR eclogites. In garnet pyrope maps (center), the

color gradient represents the range in pyrope compositions within each garnet and the range of values represented is given on the color bars in each image.

Figure 8. Proposed schematic geodynamic and metamorphic evolution of the Montagne Noire eclogites, from protolith to exhumation, showing their structural relationship and evolution withing the crustal architecture and associated metamorphic conditions (P, T, fluids). a) Schematic pre-orogenic Cambro-Ordovician setting with emplacement of mafic protolith in a thinned crust, and depth-position of protoliths within the crust; b) late orogenic crustal evolution of eclogite associated with thickening of the foreland region and deepening of the Moho, and deep crustal flow associated with distinct trajectories and magnitude of transport of dome-core and dome-margin eclogites as they reached eclogite-facies conditions from 320-310 Ma; c) exhumation of eclogites in the Montagne Noire dome and associated metamorphic conditions between 310-300 Ma. The 'flame' symbol indicates heat source at high-*P* from partially-molten migmatites and the 'water drop' symbol indicates source of fluids for zircon recrystallizing at high-*P* from partially molten migmatites and/or fluids driven off as a result of their partial melting.

Figure 9. Schematic cross section of proposed eclogite trajectories from protolith to eclogite-facies and subsequent exhumation. Dome-core O-isotope and U-Pb petrochronology data is summarized on the left, and dome-margin data is summarized on the right, showing the $\delta^{18}O$ values measured in the eclogites compared to the likely $\delta^{18}O$ signature of migmatites proposed to have variably interacted with eclogites emplaced at different locations in the dome.